1 Aerosol radiative effects in the ultraviolet, visible, and near-infrared spectral ranges using long-term

2 aerosol data series over the Iberian Peninsula

3

4 D. Mateos[1,2], M. Antón[1], C. Toledano[2], V. E. Cachorro[2], L. Alados-Arboledas[3,4], M. Sorribas[3,4,5],

5 M.J. Costa[6], J.M. Baldasano[7].

6 1. Departamento de Física, Universidad de Extremadura, Badajoz, Spain

7 2. Grupo de Óptica Atmosférica, Universidad de Valladolid, Valladolid, Spain

8 3. Departamento de Física Aplicada, Universidad de Granada, Granada, Spain

9 4. Andalusian Institute for Earth System Research, Universidad de Granada, Granada, Spain

10 5. Estación de Sondeos Atmosféricos El Arenosillo, INTA, Huelva, Spain

11 6. Évora Geophysics Centre and Dep. Physics, University of Évora, Évora, Portugal

12 7. Universidad Politécnica de Cataluña, Barcelona, Spain

13

14 Corresponding author: D. Mateos, Grupo de Óptica Atmosférica, Universidad de Valladolid, Paseo

15 Belén 7, 47011, Valladolid, Spain. E-mail: mateos@goa.uva.es

16

17

18

19

Abstract

A better understanding of the aerosol radiative properties is a crucial challenge for climate change studies. This study aims to provide a complete characterization of aerosol radiative effects in different spectral ranges within the shortwave (SW) solar spectrum. For this purpose, long-term datasets of aerosol properties from six AERONET stations located in the Iberian Peninsula (Southwestern Europe) are analyzed in term of climatological characterization and trends. Aerosol information is used as input to the libRadtran model in order to determine the aerosol radiative effect at the surface in the ultraviolet (ARE_{UV}), visible (ARE_{VIS}), near-infrared (ARE_{NIR}), and the entire SW range (ARE_{SW}) under cloud-free conditions. Over the whole Iberian Peninsula, yearly aerosol radiative effects in the different spectral ranges are: $-1.1 < ARE_{UV} < -0.7$ W m^{-2}, $-5.7 < ARE_{VIS} < -3.5$ W m^{-2}, $-2.6 < ARE_{NIR} < -1.6$ W m^{-2}, and $-8.8 < ARE_{SW} < -5.7$ W m^{-2}. The four variables showed positive statistically significant trends between 2004 and 2012, e.g., ARE_{SW} increased $+3.6$ W m^{-2} per decade. This fact is linked to the decrease in the aerosol load, which presents a trend of -0.04 unit of aerosol optical depth at 500 nm per decade, hence a reduction of aerosol effect on solar radiation at the surface is seen. Monthly means of ARE show a seasonal pattern with larger values in spring and summer. The aerosol forcing efficiency (AFE), ARE per unit of aerosol optical depth, is also evaluated in the four spectral ranges. AFE exhibits a dependence on single scattering albedo and a weaker one on Ångström exponent. AFE is larger (in absolute value) for small and absorbing particles. The contributions of the UV, VIS, and NIR ranges to the SW efficiency vary with the aerosol types. Aerosol size determines the fractions of AFE_{VIS}/AFE_{SW} and AFE_{NIR}/AFE_{SW}. VIS range is the dominant region for all types, although non-absorbing large particles cause a more equal contribution of VIS and NIR intervals. The AFE_{UV}/AFE_{SW} ratio shows a higher contribution for absorbing fine particles.

1. Introduction

Atmospheric aerosol particles can absorb and scatter part of the total amount of solar radiation entering the Earth's atmosphere. In fact, aerosols directly influence the Earth's energy budget and act as cloud condensation nuclei modifying the cloud structure (e.g., Forster et al., 2007). Aerosols can either be produced by ejection into the atmosphere or by physical and chemical processes within the atmosphere. Aerosol particles affect the radiative field by attenuating the direct component thereby enhancing (or reducing under a highly absorbing aerosol) the diffuse one. They also produce indirect effects (AIE) by perturbing the Earth's atmospheric radiative balance by modulating cloud albedo and fraction. The AIE can be viewed as a series of processes linking various variables such as aerosol mass, cloud condensation nuclei concentration, ice nuclei concentration, water phase partitioning, cloud optical properties, etc. (Penner et al., 2001).

The aerosol radiative effect (ARE) is defined as the change in net radiation due to changes in atmospheric aerosol properties and content. This is a key quantity in the determination of climate change (e.g., Hansen et al., 1998). Most studies dealing with ARE have focused on discrete wavelengths, whole shortwave (SW) solar radiation spectrum (e.g., Rajeev and Ramanathan, 2001; García et al., 2008; di Sarra et al., 2008; Cachorro et al., 2008; Foyo et al., 2014), longwave (LW) radiation (e.g., Panicker et al., 2008; di Sarra et al., 2011; Antón et al., 2014), ultraviolet (UV) interval (e.g., Hatzianastassiou et al., 2004; Kazadzis et al., 2009; Nikitidou et al., 2013), and visible (VIS) range (e.g., Jayaraman et al., 1998; Horvath et al., 2002; Bush and Valero, 2003; Meloni et al., 2003). With regards to surface SW radiative effect (ARE_{SW}), Di Biagio et al. (2010) obtained the maximum radiative daily effects for different aerosol types in the Central Mediterranean in the period 2004-2007: -61 Wm^{-2} (desert dust aerosols), -26 Wm^{-2} (urban/industrial ‑ biomass burning aerosols) and -43 Wm^{-2} (mixed aerosols). All these negative figures point out a cooling of the Earth's surface. Aerosol radiative effects in the LW (ARE_{LW}) are expected to be smaller than in the

SW and with positive sign (see, e.g., di Sarra et al., 2011; Antón et al., 2014). Hence, this heating

effect at the surface can partly offset the cooling induced in the SW range. With respect to the ARE

for the UV range (ARE_{UV}), Nikitidou et al. (2013) analyzed the ARE in two different spectral

regions in the UV range, 300-315 and 315-360 nm. They found a stronger attenuation in the UV-B

than in the UV-A, however being both solar zenith angle (SZA) dependent because of different

photon paths.

The main goal of this study is to evaluate the ARE at the surface over the Iberian Peninsula, which

is a region of great interest because of its geographical position in Southwestern Europe, near the

African continent and the interface between the Atlantic Ocean and the Mediterranean Basin. Thus,

it is affected by frequent desert dust intrusions which modulate their aerosol climatology (Toledano

et al., 2007a, Bennouna et al., 2013; Pey et al., 2013; Valenzuela et al., 2012). In addition, this area

is also affected by a great variety of air masses loaded with different aerosol types: clean

continental, polluted plumes of central Europe, and marine aerosols. Hence, aerosol climatology at

six stations (Palencia, Barcelona, Cabo da Roca, Évora, Granada, and El Arenosillo) is also carried

out for different time periods between 2001 and 2012. Aerosol radiative effects as well as their

efficiency are calculated in four regions of the solar spectrum (ultraviolet, visible, near-infrared, and

shortwave) and the relative contribution of each range with respect to the whole solar spectrum is

analyzed as a function of the aerosol properties. Therefore, this study is intended to contribute to the

understanding of the aerosol impact on radiative budget over the Iberian Peninsula.

This article presents the following outline: detailed descriptions of the aerosol stations and the

database used are performed in Section 2; Section 3 includes the followed methodology; the results

obtained in the different analyses about the climatology of aerosol properties, aerosol radiative

effects, and aerosol forcing efficiencies are shown and discussed in Sections 4,5, and 6,

respectively. Finally, the main conclusions of this article are summarized in Section 7.

92

2. Columnar aerosol optical data

The aerosol data are obtained from the Aerosol Robotic Network (AERONET) (Holben et al., 1998). Six AERONET sites operating in the Iberian Peninsula are selected in this study: Palencia, Barcelona, Évora, Cabo da Roca, Granada and El Arenosillo (see Table 1), all of them with a minimum of 8 years of data sets of continuous observations. These sites present the largest records of aerosol properties in the Iberian Peninsula in the AERONET network.

The standard instrument used in AERONET is the Cimel CE-318 radiometer. It performs direct sun measurements at several wavelengths in the spectral range 340-1020 nm. Furthermore, the instrument also measures sky radiance in the solar almucantar and principal plane configurations at 440, 670, 870 and 1020 nm wavelengths. A detailed description of this instrument was provided by Holben et al. (1998). The direct sun observations are used to derive the spectral aerosol optical depth (AOD) and the corresponding Ångström exponent. The sky radiances together with the AOD are employed to retrieve a set of aerosol optical and microphysical properties via inversion methods (Dubovik and King, 2000; Dubovik et al., 2006). These include particle size distribution, complex refractive index, single scattering albedo (SSA), phase function, asymmetry parameter, fraction of non-spherical particles, etc. (see http://aeronet.gsfc.nasa.gov/new_web/Documents/Inversion_products_V2.pdf). Data are provided in three database levels: 1.0 (raw data), 1.5 (cloud-screened) and 2.0 (cloud-screened and quality assured).

The calibration of these instruments is performed following AERONET protocols by AERONET-NASA, PHOTONS and RIMA networks every 12 months of operation approximately. The estimated uncertainty is 0.01-0.02 for AOD (larger at shorter wavelengths) and ~5% for the sky

115 radiances (Holben et al., 1998). The SSA has an absolute uncertainty about 0.03-0.07 depending on

116 the aerosol load and type (Dubovik et al., 2000).

117 Level 2.0 aerosol optical depth data have been used in this work. However, it is well-known that

118 when level 2.0 inversion data are used, the number of available observations of single scattering

119 albedo (SSA) and asymmetry factor (g) is quite limited because these variables are only considered

120 reliable when $AOD_{440nm} > 0.4$[1]. Such AOD is mainly reached in the study region during Saharan

121 dust or biomass burning events, therefore we would not have information on SSA and g for other

122 conditions. To solve this issue, we have reduced the threshold of the level 2.0 inversion products.

123 For this, we started with the level 1.5 data (for those quality-assured almucantar data that reached

124 level 2.0) and applied the same criteria used by AERONET to elaborate the level 2.0 regarding the

125 number   of   symmetrical   angles,   retrieval   error   and   solar   zenith   angle   (see

126 http://aeronet.gsfc.nasa.gov/new_web/Documents/AERONETcriteria_final1_excerpt.pdf).

127 However, a less restrictive threshold is applied to the AOD, which we restricted to cases with

128 $AOD_{440nm} > 0.15$, instead of 0.4. This choice must be considered a compromise between the amount

129 and the quality of the data. This kind of approach has been adopted by other authors using

130 AERONET absorption data (e.g. Mallet et al., 2013). The threshold of 0.15 seems adequate

131 analyzing the typical values of the AOD in the Iberian Peninsula (e.g., Bennouna et al., 2011;

132 Obregón et al., 2012), because it can be considered a value to separate background aerosol

133 conditions from episodic events with moderate or high aerosol loadings. The level 1.5-filtered data

134 of SSA and g are daily averaged in order to have one value per day. In these conditions, the

135 estimated uncertainty of the single scattering albedo is ±0.05-0.07 (Dubovik et al., 2000).

136 Furthermore, for those days presenting level 2.0 data but also measurements in the 1.5-filtered level,

137 we tested the uncertainty of our approach. We evaluated the difference in the SSA values of the

---

[1] Other inversion products, like the volume size distributions, are provided for all AOD levels.

138 level 1.5-filtered data with respect to the closest level 2.0 data. The mean relative differences in the

139 SSA values between both methodologies are smaller than 1%, being in the same order that the

140 inversion uncertainty.

141 Lastly, when the AOD is low (<0.15 at 440 nm), there is no reliable information on the absorption

142 properties in the almucantar retrievals. Such low AOD is typical in our study region (e.g. almost

143 70% of observations at Palencia, Granada and Évora are below this threshold). If only cases with

144 AOD_{440nm}>0.15 are considered in our study, the derived aerosol radiative effect would be

145 unrealistically large. To overcome this problem of representativeness, fixed values of SSA (0.90)

146 and g (0.75) have been used for the cases with AOD < 0.15 at 440 nm, considering typical values

147 for continental, desert, and maritime aerosols (e.g., Hess et al., 1998). In spite of the associated

148 uncertainties, our approximation (daily level 1.5-filtered values of these aerosol properties for AOD

149 > 0.15 together with a typical fixed value for low AOD cases) provides a good characterization of

150 the aerosol absorption of the particles present in the atmosphere. The data products and AERONET

151 database level are summarized in Table 2, where the estimated absolute uncertainties of AOD and

152 SSA are also provided.

153

154 **3. Methodology**

155 The ARE calculations are performed in the ultraviolet (ARE_{UV}, 280-400 nm), visible (ARE_{VIS}, 400-

156 700 nm), near-infrared (ARE_{NIR}, 700-2800 nm), and shortwave (ARE_{SW}, 280-2800 nm) intervals.

157 For this purpose, cloud-free simulations are carried out by means of a radiative transfer code.

158 The libRadtran model (Mayer and Kylling, 2005) has been shown to be a useful tool for obtaining

159 solar radiation data, presenting high accuracy in both cloudy and overcast conditions (e.g., Mateos

160 et al., 2013b, 2014; Román et al., 2014). Version 1.7 of the libRadtran is used in this study with

inputs of aerosol, total ozone column (TOC), precipitable water vapor column (PWC), and surface albedo data. We performed simulations of ultraviolet (280-400 nm), visible (400-700 nm), near-infrared (700-2800 nm), and shortwave (280-2800 nm) radiation during the periods indicated in Table 1. Total ozone column is provided by the Ozone Monitoring Instrument (OMI) and Total Ozone Mapping Spectrometer (TOMS). Daily values of these instruments are obtained from the Daily Level 3 Global Gridded products, which are downloaded using the Giovanni application (http://disc.sci.gsfc.nasa.gov/giovanni). Level 2.0 AERONET PWC data are used in the calculations. The uncertainty of this parameter is 10-15% (Holben et al., 1998). In addition, retrievals of surface albedo at 440, 675, 870 and 1020 nm from the AERONET algorithm are also used in this work. For land surface cover, this algorithm relies on the Lie–Ross model (Lucht and Roujean, 2000), but considering the bidirectional reflectance distributions from MODIS (Moody et al., 2005).

Aerosol properties obtained from AERONET measurements are also used as input to the libRadtran model. Ångström coefficients, α and β, are utilized to compute a spectral aerosol optical depth in the wavelengths of interest (Schuster et al., 2006). Ångström exponent α is obtained with the measurements between 440 and 870 nm, while the turbidity β is obtained from the α value and aerosol data at 1020 nm. Since the aerosol asymmetry factor, single scattering albedo, and surface albedo are obtained at four wavelengths from AERONET in each measurement, three different spectral regions are simulated with the libRadtran model. For computations in the UV range (280-400 nm), the AERONET retrievals of aerosol asymmetry factor, aerosol single scattering albedo, and surface albedo at 440 nm are used. The AERONET retrievals at 675 nm of the same variables are used in the visible range (400-700 nm), while in the near-infrared region (700-2800 nm) we used the average properties retrieved at 870 and 1020 nm. In each interval, these properties are considered as wavelength independent. This choice to perform the radiative transfer simulations is proven as adequate in the Appendix A. Other options in the model set-up are: extraterrestrial

186   irradiance values are taken from Gueymard (2004); profiles of temperature, air density, ozone and

187   other atmospheric gases are taken from the midlatitude summer/winter standard atmospheres; and

188   the radiative equation solver is the improved version of the discrete ordinate method of Stamnes et

189   al. (2000) (DISORT2) calculated by 16-streams (e.g., de Miguel et al., 2011). After computing the

190   solar irradiance in the different spectral intervals, the SW irradiance is evaluated by adding up the

191   contributions of these three spectral regions.

192   In order to evaluate the aerosol radiative effect, the simulations under aerosol-free conditions are

193   also computed with the same inputs as explained above, but with a fixed β value of 0.001.

194   The use of radiative transfer models fed with reliable experimental aerosol data to determine the

195   ARE has been also employed in other studies (e.g., Barja and Antuña, 2011; Valenzuela et al.,2012;

196   García et al., 2014).

197   Once the simulated radiometric values are obtained, ARE is derived for each interval (X represents

198   UV, VIS, NIR, and SW) at the surface by:

199

200      $$ARE_X = \left(X_{aer}^{\downarrow} - X_{aer}^{\uparrow} \right) - \left(X_{NOaer}^{\downarrow} - X_{NOaer}^{\uparrow} \right) \qquad\qquad (1)$$

201

202   where X_{aer} and X_{NOaer} are the irradiances (W m^{-2}) for the X range under actual and aerosol-free

203   conditions, respectively.

204   Daily values are obtained by the integration of the hourly data during the whole day (24 h)

205   considering ARE = 0 Wm^{-2} for SZA > 90º (e.g., Bush and Valero, 2003; Valenzuela et al., 2012)

206   and assuming cloud-free conditions along the day:

207

$$\text{ARE}_{\text{daily}}= \sum \text{ARE}_{\text{hourly}} \frac{dt}{24} \qquad (2)$$

208

215 With respect to the temporal trends calculated in this study, the Sen's method (Sen, 1968) is applied

216 to evaluate the slope of a time series using the Mann-Kendall non parametric test to determine the

217 significance of these rates. The Sen's method is not greatly affected by outliers and can be

218 computed when there are gaps in the database (Collaud Coen et al., 2013). This is a common and

219 adequate method in temporal trend evaluation (e.g., Sánchez-Lorenzo et al., 2013). The trends

220 calculated in this study are obtained in the corresponding physical units per year. However, to unify

221 notation with previous studies dealing with the radiative effect trends of clouds and aerosols (e.g.,

222 Mateos et al., 2013a), the results are multiplied by 10 and expressed in physical units per decade. In

223 this way, the trends are also easier to read.

224

225 **4. Analysis of aerosol properties over the Iberian Peninsula**

226 A direct CIMEL retrieval (AOD at 440 nm) is selected to perform the climatological analysis

227 because the estimations of AOD_{500nm} (used in the ARE calculations) are obtained using α values.

228 Hence, we minimized the impact of other uncertainty sources in the AOD analysis. Besides, the

229 results for AOD_{440nm} and AOD_{500nm} do not differ excessively. In order to identify the differences in

230   the aerosol climatology over the six sites analyzed in this study, the monthly distribution of the

231   daily values of the AOD_{440nm} and α are evaluated using the database mentioned in Table 1. All the

232   available level 2.0 AERONET measurements are used in this section.

233   Figure 1 shows the climatology of the aerosol load by box whisker plots. Several conclusions can

234   be drawn from this figure. The highest values of the AOD occur in Barcelona, as can be expected

235   because it is a large city. With respect to the monthly average values (triangles in the figure), the

236   central stations in the Iberian Peninsula (Palencia and Évora) exhibit AOD_{440nm} below 0.2, while the

237   southern sites (Cabo da Roca, Granada, and El Arenosillo) show aerosol load over 0.2 during

238   summer months. The AOD_{440nm} seasonal distribution is seen, with maximum values in summer and

239   minimum ones in winter. However, the seasonality becomes more evident in the stations outside the

240   central area of the Iberian Peninsula. The large differences between median and average values for

241   some months evidence a large impact of high aerosol optical depth events on the monthly

242   climatology. In this line, the bimodality of the monthly AOD climatology (with two maximum

243   monthly means occurring in March and summer months) observed for the El Arenosillo site has

244   been already reported by previous studies (e.g., Bennouna et al., 2011), and directly attributed to

245   desert dust intrusions from the African continent.

246   To go further in the characterization, α allows for a better understanding of the particle size over

247   each site. Figure 2 shows the climatology of this variable over the six stations using also box

248   whisker plots. Analyzing the monthly average means, α values larger than one, indicative of the

249   predominance of fine particles, are dominant over Barcelona, Palencia, and Évora. The other three

250   stations (Cabo da Roca, Granada, and El Arenosillo) present monthly α averages over and below 1,

251   which means a larger variety of aerosol sizes over these stations. A seasonal dependence over

252   Granada site is seen, with winter months dominated by fine particles (see also Lyamani et al., 2012)

253   and summer months by larger ones (see also Navas-Guzman et al., 2013). Values of α present a

11

254   large variability during summer which is indicative of the influence of different aerosol types

255   including biomass burning events and Saharan dust transport (e.g., Pérez-Ramírez, 2008). The

256   monthly distribution of α is symmetric with similar average and median values through the year for

257   the six sites.

258   With the daily AOD and α values, it is possible to classify the origin of the aerosol particles.

259   Previous studies suggest different thresholds of AOD and α (e.g., Hess et al., 1998; Pace et al.,

260   2006; Toledano et al., 2007b). A simple classification, which can be used for the whole Iberian

261   Peninsula, of aerosol type is carried out in this study. The threshold between fine and large particles

262   is placed at $\alpha = 1$, while the situations with a high aerosol load are those with $AOD_{440nm} > 0.2$.

263   Therefore, aerosol particles can be classified in four types: maritime ($AOD_{440nm} < 0.2$ and $\alpha < 1$),

264   desert dust ($AOD_{440nm} > 0.2$ and $\alpha < 1$), continental clean ($AOD_{440nm} < 0.2$ and $\alpha > 1$), and

265   continental polluted ($AOD_{440nm} > 0.2$ and $\alpha > 1$). Note that the limit of $AOD_{440nm} < 0.2$ is arbitrary

266   and this value could be adjusted according to the sites, which likely produce a different distribution

267   different distribution in the pie diagrams. Actually, even close stations can present slight differences

268   in the α-AOD classification (see, e.g., Obregón et al. 2012). However it is not the aim of this work

269   to provide an extensive aerosol climatology, but rather to demonstrate the great variety of air

270   masses over Iberia which transport different aerosol types. Although other types, such as biomass

271   burning or mixed aerosols, are placed in the boundaries of these types, this simple classification can

272   provide information about the aerosol sources for the six sites. The classification used here is line

273   with the previous studies. For instance, Toledano et al., (2007) proposed for El Arenosillo site

274   similar thresholds (see their Table V), although they identified continental polluted aerosols with an

275   AOD_{440nm} larger than 0.35 and $\alpha > 1.4$. Pace et al., (2006) proposed at Lampedusa island (Central

276   Mediterranean) a desert dust identification when $AOD_{440nm} \geq 0.15$ and $\alpha \leq 0.5$.

Figure 3 shows pie diagrams with the frequency of occurrence of the four aerosol types. The six diagrams agree pointing at continental clean as the main type of aerosols over the Iberian Peninsula. In Barcelona, there is also an important contribution of continental polluted, since Barcelona is a large coastal city with relevant pollution levels from vehicular and ship traffic (e.g., Reche et al., 2011). The influence of maritime aerosols is notable at El Arenosillo, Cabo da Roca, and Évora sites (Toledano et al., 2007a, Bennouna et al., 2011; Obregón et al., 2012). Furthermore, desert dust events are shown to be common in the Iberian Peninsula with a higher occurrence at Granada and El Arenosillo sites (the two closest points to the African continent and hence to the Saharan desert) (see also Toledano et al., 2007; Guerrero-Rascado et al., 2008; Antón et al., 2012b). For instance, the minimum values of α obtained for Granada station during summer months are linked to the higher likelihood of desert dust events (Valenzuela et al., 2012), being sometimes associated with high aerosol loads (Córdoba-Jabonero et al., 2011). These results corroborate the findings obtained by previous studies about desert dust events over the Iberian Peninsula (see, e.g., Lyamani et al., 2005; Cachorro et al., 2006; 2008; Toledano et al., 2007b).

The temporal trend of aerosol load can be established over the last decade in the Iberian Peninsula. The yearly values of AOD_{440nm} at the six sites are shown in Figure 4. The geographical distribution of AOD through the Spanish geography is observed in the figure. Barcelona site presents yearly values over ~0.2. Granada, El Arenosillo, and Cabo da Roca exhibit yearly means in the interval between 0.15 and 0.22, while the means for Palencia and Évora sites are slightly lower in the range 0.12-0.18. Analyzing the six sites together, the year of 2010 presents one of the minimum values of AOD_{440nm}, while the maximum averages seem to appear at the early 2000s. The different sampling of AOD measurements in the six sites can produce discrepancies because different events are or are not captured in each database. Looking at the years with a large sampling (>200 days in, at least, four stations), 2005, 2007, and 2011, all the features mentioned above are corroborated for these particular years. The minimum of 2010 occurs when two Southern sites (El Arenosillo and Cabo da

13

Roca) have not enough data to evaluate the yearly mean. Hence, we cannot ensure that the apparent minimum of AOD recorded that year is linked to global-scale phenomena or to more local conditions at the other sites. During 2010 a persistent negative phases of North Atlantic Oscillation (NAO) and Quasi Biennal Oscillation (QBO) indexes was observed (e.g., Steinbrecht et al., 2011), and the connection between air mass transport at global scale and particulate matter (at the surface) is proved by Pey et al., (2013) in the Eastern Iberian Peninsula.

With respect to the temporal trend rates, the evolution of these yearly values seems to be weak. The evaluation of the trend rates (Mann-Kendall test with the 95% significance level) only produces one statistically significant trend for the Barcelona site, where a decrease of the aerosol load of 0.09 AOD_{440nm}-unit per decade is observed. Although the results obtained for the other sites are not statistically significant, the sign of the temporal trends is negative for all of them. In particular, Évora and Palencia stations showed trend rates of -0.06 and -0.04 AOD_{440nm}-unit per decade with significance levels of 94% and 90%, respectively. Hence, a slight reduction of the aerosol load over the Iberian Peninsula is observed since 2000. This result obtained in the Southeastern Europe is in line with the long-term analysis of AOD series performed in Northern Germany and Switzerland by Ruckstuhl et al. (2008). These authors highlight a strong decrease of aerosol load starting in 1985, while the values are stabilized since about 2000.

The reasons behind the decrease in the aerosol load since the early 2000s are a mixed of anthropogenic and natural sources. As was reported by Aas et al. (2013), the particulate matter (PM) emissions in the Iberian Peninsula have decreased around 25% between 2000 and 2011. Furthermore, observational PM data in different Spanish sites have also shown a decrease trend in the 2000s (e.g., Barmpadimos et al., 2012; Cusack et al., 2012; Pey et al., 2013; Bennouna et al., 2014). This fact can be understood by the effect of the current economic crisis and the implementation of new environmental laws to control the pollution (e.g., Querol et al., 2014). In

addition, recent studies have shown that natural aerosols have also decreased in the last decade. For instance, Gkikas et al. (2013) reported, using satellite AOD estimations, that strong and extreme desert dust episodes in the Mediterranean decreased in the period 2000-2007 over land surfaces. This trend is understood due to the low spring and summer frequencies in 2005 and 2007 and the high frequencies in 2000 and 2003. As it was shown by Pey et al. (2013), one possible reason behind this trend is the atypical trajectories followed by the air masses emerging from North Africa in summer since 2006. Hence, both columnar and surface aerosols have pointed out a decrease in the aerosol load concerning both anthropogenic and natural aerosols.

5. Inter-annual and intra-annual evolution of ARE

From the daily data, the yearly ARE for each station and spectral range are evaluated to analyze their inter-annual changes (see Figure 5). In spite of the high variability of the yearly values with large standard deviations (see the vertical bars for Palencia station in the figure), the radiative effects of atmospheric aerosols have slightly declined over the last years. The patterns of ARE in the UV, VIS, NIR, and SW ranges are similar, since the inter-annual changes are simultaneously observed in the four spectral intervals. The significance levels of the temporal trends (Mann-Kendall nonparametric test at the 95% confidence interval) are evaluated. Évora and Palencia sites exhibit statistically significant trends in the periods 2005-2012 and 2003-2012, respectively. The trends for the aerosol effects for Palencia (Évora) are: +4.9 (+3.2) Wm^{-2} per decade in ARE_{SW}, +3.3 (+2.1) Wm^{-2} per decade in ARE_{VIS}, +0.1 (+0.08) Wm^{-2} per decade in ARE_{NIR}, and +0.06 (+0.03) Wm^{-2} per decade in ARE_{UV}. The other four stations present positive trends in all the spectral ranges, but they are not statistically significant at the 95% confidence interval. The decrease in the aerosol effects is in line with the previous fall in the AOD values in the 2000s mentioned in Section 4. Furthermore, this slight reduction in the radiative effects of the atmospheric aerosol over the Iberian

15

Peninsula could partially contribute to the increase in the levels of SW radiation at the surface (the brightening phenomenon) in this region reported by Sanchez-Lorenzo et al. (2013) and Mateos et al. (2013a).

To establish the general behavior of the ARE over the whole Iberian Peninsula, the yearly values using the six ground-based stations are evaluated. Only those years with, at least, simultaneous measurements at three sites are considered in these averages, and consequently, the time period is limited to 2004-2012. Figure 6 shows the evolution of the ARE and AOD at 500 nm for the entire peninsula. The previously discussed reduction of aerosol load in the six individual datasets is again corroborated with the mean data series. This decline produces a consequent decrease in the aerosol radiative effect at the four spectral ranges. The temporal trends of these yearly values are evaluated, and all the trends resulted statistically significant at the 95% significance level are shown in Figure 6. Overall, ARE_{SW} over the Iberian Peninsula increased 3.6 W m^{-2} per decade while the aerosol reduced 0.04 AOD_{500nm}-unit per decade. The yearly aerosol radiative effects over the entire peninsula are in the ranges: $-1.1 < ARE_{UV} < -0.7$ W m^{-2}, $-5.7 < ARE_{VIS} < -3.5$ W m^{-2}, $-2.6 < ARE_{NIR} < -1.6$ W m^{-2}, and $-8.8 < ARE_{SW} < -5.7$ W m^{-2}. The larger contribution of the visible spectral region with respect to the whole solar spectrum was also noticed by Bush and Valero (2003). The relationship between ARE and AOD_{500nm} is analyzed more in detail in Section 6, when the aerosol forcing efficiency is evaluated for each ground-based station.

In addition to the inter-annual changes, the intra-annual behavior is also analyzed. For this purpose, the annual cycle (12 monthly means) is evaluated for the six stations (see Figure 7). A seasonal pattern is seen in ARE_{UV} and ARE_{VIS}, and therefore, ARE_{SW}. However, ARE_{NIR} does not follow a seasonal pattern, particularly at the Évora and Palencia stations given that ARE_{NIR} remains nearly constant. Small differences among the six stations are observed in the annual cycle during the cold seasons. The aerosol radiative effects are stronger during summer months. This can be related to the

higher likelihood of desert dust or biomass burning events over the Iberian Peninsula in these months (e.g., Cachorro et al., 2008; Valenzuela et al., 2012), as was mentioned above. This is corroborated by the increase of the differences among the stations during the warm season, likely due to the variability in the impact of the desert dust episodes which strongly depend on the geographical location of each site. The higher occurrence of large aerosol loads during the warm seasons (see Figure 1), can explain the more negative ARE during summer and spring in Figure 7. For instance, the Barcelona station, with the largest values of AOD_{440nm}, is the bottom curve of each panel in Figure 7. Furthermore, the influence of mineral dust aerosol (with high aerosol optical depth) during these months also causes strong radiative effects, as was also reported by previous studies (e.g., Cachorro et al., 2008; Guerrero-Rascado et al., 2009; Antón et al., 2012a, 2012b; Román et al., 2013; García et al., 2014). In addition, the bimodality of the monthly AOD climatology mentioned in Section 4 has its impact on the radiative effects. The annual AOD cycle (see Figure 1, El Arenosillo site) causes the inverse monthly distribution of ARE with a first minimum in March. This effect is more clearly seen in ARE_{NIR} and ARE_{SW}.

6. Aerosol radiative forcing efficiency in different spectral ranges

The daily AFE values are calculated (following the methodology described in Section 3) in all the spectral ranges. AFE is a function of the aerosol optical properties, where both the aerosol particle size distribution and absorptive properties play a key role (e.g., Antón et al., 2011). As we assumed a fixed value of SSA = 0.90 in the simulations with $AOD_{440nm} < 0.15$ (see Table 2), the AFE is calculated only for those cases showing AOD_{440nm} larger than 0.15.

To identify the influence of SSA and α on AFE, this variable is calculated for several intervals of each aerosol property. Four categories of single scattering albedo at 675 nm are established in the calculation of the AFE: $1.0 \geq SSA_1 > 0.95$, $0.95 \geq SSA_2 > 0.90$, $0.90 \geq SSA_3 > 0.85$, and $0.85 \geq$

17

398    $SSA_4 > 0.80$. Furthermore, aerosol size is classified in three intervals: $0 \leq \alpha_1 \leq 1$, $1 < \alpha_2 \leq 1.5$, and

399    $1.5 < \alpha_3 \leq 2$. Note that two intervals in the range of α larger than 1 have been considered. One for

400   median particles and another one for fine particles, because of the relevant importance of median

401   size particle (continental or mixed aerosol aerosols types) over the Iberian Peninsula (see Figure 3).

402   Although the general classification between fine and coarse particles requires a more refined

403   classification (Schuster et al.,2006; Prats et al., 2011), the more general intervals selected in this

404   study are adequate to perform a study of the aerosol sizes at the six stations together.

405   Figure 8 shows the AFE obtained for the UV (AFE_{UV}), VIS (AFE_{VIS}), NIR (AFE_{NIR}), and SW

406   (AFE_{SW}) ranges for all these intervals. The threshold to evaluate the average in each sub-interval is

407   fixed at 10 data points. From these figures it is seen that, the stronger the absorption by aerosols, the

408   stronger their forcing efficiency. That is a decrease in the absolute values of the AFE for increasing

409   SSA and for all particle size. In general, the groups of non-absorbing particles exhibit a good

410   agreement among the six stations (see, for instance, AFE values in all the spectral ranges in the

411   interval $1 < \alpha \leq 1.5$). Larger differences are obtained in the case of more absorbing aerosol particles.

412   These can be understood because of the different types of aerosols presented over each site (see

413   Section 4) and the different data numbers. The average AFE values over the whole Iberian

414   Peninsula (considering the six stations together) are presented in Table 3 as a function of α and

415   SSA, separately. The role played by the aerosol size on AFE values is different in the three sub-

416   intervals of the shortwave radiation. AFE_{UV} and AFE_{VIS} are larger (in absolute value) for fine

417   particles, while the opposite occurs in the case of AFE_{NIR}. As a result of these mixed effects, AFE_{SW}

418   shows also a decrease in its values with increasing α, but this effect is weaker than for the visible

419   and ultraviolet parts. SSA exhibits a more dominant role. As was observed before, the most

420   negative values are achieved for the most absorbing aerosols considered in this study (group 1 of

421   SSA, see Table 3).

422   The average values of forcing efficiency obtained in this study (see Table 3) are in line with those

423   found by other authors. Table 4 summarizes the results obtained by previous studies. It is difficult to

424   assess some features in the comparison with previous reported AFE values, because of the different

425   aerosol types, time periods and methods that are analyzed. Our study presents the evaluation of

426   ARE with six long-term databases of aerosol properties. In spite of that, the values shown in Table

427   3 agree with those of Table 4, but the larger discrepancies are observed with the studies focusing on

428   specific events. Our results match better with the results reported by, e.g., Zhou et al. (2005),

429   Meloni et al. (2005), and Di Biagio et al. (2010). As was noticed by, e.g., Costa et al. (2004, 2006)

430   and Di Biagio et al. (2010), AFE at the surface is larger (in absolute term) for aerosols characterized

431   by smaller and absorbing particles. This result is corroborated by the findings shown in this study.

432   Furthermore, as was pointed out by Di Biagio et al. (2010), the aerosol absorption is the dominant

433   factor on AFE evaluated at the surface.

434   To evaluate the contribution of each spectral range with respect to the shortwave, the dependence of

435   each AFE ratio (VIS to SW and NIR to SW) on SSA and α is shown in Figure 9. AFE_{VIS}/AFE_{SW}

436   and AFE_{NIR}/AFE_{SW} ratios are shown in the figure since their contributions are the dominant.

437   AFE_{UV}/AFE_{SW} ratio can be obtained as 100% minus the sum of the percentage of the two other

438   ranges. As expected, non substantial differences are observed in the behavior of the six stations

439   considered in this study. The NIR contribution becomes more decisive for large particles ($\alpha < 1$). It

440   is expected that larger particles interact more with the longer wavelengths, while the smaller

441   particles present more interaction with the shorter wavelengths. The presence of large particles with

442   low SSA (high absorption) leads to a reduction of the AFE_{NIR}/AFE_{SW} ratio as well as an increase of

443   the AFE_{VIS}/AFE_{SW} ratio. However, for non-absorbing (high SSA) large particles, the

444   AFE_{NIR}/AFE_{SW} ratio increases, and the contributions of the visible and infrared parts become more

445   similar (both around ~40-50%). The difference between AFE_{VIS}/AFE_{SW} and AFE_{NIR}/AFE_{SW}

446   increases for intermediate - fine particles. For these particles, the AFE_{VIS}/AFE_{SW} ratio does not

447 show a dependence on SSA. The smallest contribution of the NIR interval is around ~25% under

448 strong absorbing aerosols and fine particles, while AFE_{VIS}/AFE_{SW} is still over 60%. For this case,

449 the contribution of the ultraviolet range achieves a maximum of ~15%, being almost comparable

450 with the near infrared contribution. In summary, aerosol size determines the relevance of VIS-NIR

451 ranges, while SSA plays a key role, particularly, for large particles.

452

7. Conclusions

454 Six long-term datasets of aerosol properties over the Iberian Peninsula were analyzed and used as

455 input in a radiative transfer model to simulate ultraviolet, visible, near-infrared, and shortwave

456 radiation. The aerosol radiative effect (ARE) and aerosol forcing efficiency (AFE) were calculated.

457 The main conclusions are as follows:

458 1) The annual cycles of AOD and α values of atmospheric aerosols over the six analyzed stations

459 present high variability among them, emphasizing the inhomogeneity of the Iberian Peninsula,

460 mainly due to the different aerosol types over each station. The Barcelona site presents the largest

461 values of AOD, although Southern stations (Granada and El Arenosillo sites) frequently exhibit

462 daily values over 0.2 during summer months. The classification α-AOD has shown that continental

463 (mainly, clean) is the principal type of aerosol over the Iberian Peninsula. However, maritime

464 aerosols are also common in the Cabo da Roca, El Arenosillo and Évora sites. Desert dust events

465 are registered at the six sites, with the highest frequency at Granada and El Arenosillo, but the most

466 relevant feature is the South-North gradient of desert dust load which modulates the aerosol

467 climatology over the Iberian Peninsula.

468 2) The aerosol load over the Iberian Peninsula has shown a decrease trend between 2004 and 2012

469 (-0.04 per unit of AOD_{500nm} per decade, being statistically significant at the 95% of significance

470   level). Yearly values of the AOD at 440 nm have also shown a statistically significant trend of -0.09

471   AOD_{440nm}-unit per decade at Barcelona site. The temporal trends for the rest of the stations are not

472   statistically significant at the 95% significance level, but all of them are negative. Hence, a

473   reduction of the aerosol column load over the Iberian Peninsula is observed in the last decade.

474   3) In the whole Iberian Peninsula, yearly ARE_{UV} ranges between -1.1 and -0.7 Wm^{-2}, ARE_{VIS}

475   ranges between -5.7 and -3.6 Wm^{-2}, and ARE_{NIR} has values between -2.6 and -1.6 Wm^{-2}. As a

476   result, ARE_{SW} is in the range between -8.8 and -5.7 Wm^{-2}. The temporal trends of ARE_{UV}, ARE_{VIS},

477   ARE_{NIR}, and ARE_{SW} exhibit positive statistically significant trends between 2004 and 2012. For

478   instance, the trend rate for the ARE_{SW} is +3.6 Wm^{-2} per decade (statistically significant at the 95%

479   of significance level).

480   4) The intra-annual ARE cycle exhibits larger values during the spring and summer months when

481   the likelihood of high aerosol loading over the Iberian Peninsula increases. In general, the annual

482   AOD cycle is driven by the occurrence of Saharan dust events.

483   5) The AFE values at the six stations used in this study are in good agreement. Conditions of high α

484   (small particles predominate) and low SSA (high absorption) lead to the largest negative AFE

485   values. Overall, as an average for the Iberian Peninsula: AFE_{UV} = -6 $Wm^{-2}\tau^{-1}$, AFE_{VIS} = -34 $Wm^{-2}\tau^{-1}$

486   , AFE_{NIR} = -19 $Wm^{-2}\tau^{-1}$, and AFE_{SW} = -59 $Wm^{-2}\tau^{-1}$.

487   6) The contribution of the ultraviolet, visible, and infrared to total shortwave aerosol forcing

488   efficiency is governed by the aerosol type. In general, the visible part of the spectrum is the most

489   dominant part. Non-absorbing large particles cause a more equal contribution of VIS and NIR

490   intervals, while the UV range shows a higher contribution for absorbing fine particles.

491

492

Appendix A

The two choices in the performance of radiative transfer simulations from the libRadtran code concerning aerosol properties are justified in this section.

First at all, as it is mentioned in the text, most of the data present $AOD_{440nm} < 0.15$ (~70% for Palencia, Granada, and Évora sites). For these low values, $SSA = 0.9$ and $g = 0.75$ are selected by the representativeness of the local aerosols in the six sites of study. To analyze possible uncertainties emerging from this choice, Table A1 shows the relative difference between two extreme cases of SSA ($SSA_1 = 0.8$ and $SSA_2 = 1.0$) for different values of the asymmetry factor and two different SZAs (30º and 60º). The two optical properties are also fixed as non-wavelength-dependent in this analysis. The AOD_{440nm} used is 0.15, the worst scenario possible for these cases because the higher the AOD the stronger the impact of aerosol properties. The simulations are performed for the four spectral ranges, and the net flux at the surface is evaluated for all of them. The change of SSA between the two extreme cases produce a relative difference in the SW range less than 5%, the relative difference is higher for the UV range but also <10%. Furthermore, as the SSA influences the diffuse radiation, the worst results are obtained at large SZAs. The impact of g on the net fluxes is very weak. In conclusion, the choice of $SSA = 0.9$ and $g = 0.75$ in a clean scenario ($AOD_{440nm} < 0.15$) is proven as adequate because of two reasons: a) representativeness of the local aerosols which can be mixture of different types, and b) the low uncertainty produced in the simulations by SSA and g under these conditions.

The choice of fixed SSA and g values within each of the spectral ranges (UV, VIS, and NIR) represented by the CIMEL spectral measurements is also justified here. The aerosol models by Shettle (1989) included in the libRadtran code (see Mayer and Kylling, 2005) are used to evaluate the uncertainty of using this approximation. The continental clean aerosols (most common type in the Iberian Peninsula, see Figure 3), and continental polluted aerosols (also very common, which

present an extreme case of absorption) are tested in this analysis. The simulations are performed for the expected spectral behavior of SSA and g following Shettle (1989) and the case of fixed properties in the UV (SSA and g values at 440 nm), VIS (SSA and g values at 675 nm), and NIR intervals (SSA and g average of values at 870 and 1020 nm). Figure A1 presents the evolution of the relative error (considering as reference the net flux with the expected spectral dependence of aerosol properties) for several AOD values between aerosol-free and $AOD_{550nm} = 0.6$. In the case of continental clean aerosols (Figure A1.a), the error of using our assumption is lower than 5% for all SZAs and spectral ranges. Therefore, as the large majority of aerosol particles are of this type, the methodology used and proposed in this study only introduces a relative error below 5% in the majority of the simulations. With respect to the continental polluted aerosols (Figure A1.b), the error increases achieving a maximum around 20% for the UV range and very turbid conditions. For large AOD conditions in the Iberian Peninsula (e.g., $AOD_{550nm} = 0.4$) but with low frequency of occurrence in contrast to $AOD_{440nm} < 0.15$, the error of the SW range is below 5%. However, the UV range is more sensitive to our method and the error is around 15% at SZA = 60º. As it was mentioned above, the errors are larger for large SZAs because of the possible interaction between absorption and scattering processes resulting the diffuse radiation. The visible range is more sensitive to the spectral variations than the NIR interval, which exhibits a maximum error around 11% at SZA = 60º and $AOD_{550nm} = 0.6$. The daily net radiative fluxes are also evaluated for the two aerosol types in order to quantify the uncertainty in the final simulated data used in this study. For Palencia site (and the corresponding SZA evolution), a daily value for the June 20th is simulated assuming TOC = 300 DU and PWC = 1 cm. The results for the continental polluted case with $AOD_{440nm} = 0.4$ exhibit differences between the spectral and fixed-band aerosol properties of: 7.5%, 5.3%, 4.0%, and 4.8% for the UV, VIS, NIR, and SW intervals. The relative errors for the same intervals with continental clean (and same AOD value) are: 1.9%, 1.2%, 1.4%, and 1.4%, respectively. Therefore, the uncertainty due to fixed optical properties in each spectral range is

dependent on the aerosol type but the error caused can be considered as acceptable. Since actual aerosols often present mixtures of different types, the uncertainty of using the theoretical spectral evolution for one type (given by an aerosol model) can also produce uncertainties which should be taken into account. Although other aerosol types are not tested in this analysis, a similar behavior can be expected. For instance, for the case of desert dust aerosols, Román et al. (2013) found a slight influence of spectral aerosol absorption properties on UV irradiance analyzing a strong Saharan intrusion over Granada site.

Therefore, the two assumptions performed in this study in the simulations are adequate for the evaluation of net fluxes and aerosol radiative effects. The uncertainties that can be introduced in the daily values are acceptable being around or smaller than 5% for the net SW radiation. This uncertainty is usually achieved in clear-sky modeling (e.g., Mateos et al., 2010; Bilbao et al., 2011).

References

Aas, W., Espen Yttri, K., Stohl, A., Lund Myhre, C., Karl, M., Tsyro, S., Marečková, K., Wankmüller, R., Klimont, Z., Heyes, C., Alastuey, A., Querol, X., Pérez, N., Moreno, T., Lucarelli, F., Areskoug, H., Balan, V., Cavalli, F., Putaud, J.P., Cape J.N., Catrambone, M., Ceburnis, D., Conil, S., Gevorgyan, L., Jaffrezo, J.L., Hueglin, C., Mihalopoulos, N., Mitosinkova, M., Riffault, V., Sellegri, K., Spindler, G., Schuck, T., Pfeffer, U., Breuer, L., Adolfs, D., Chuntonova, L., Arabidze, M., and Abdulazizov, E.: Transboundary particulate matter in Europe Status report 2013, EMEP Report, 4/2013 (Ref. O-7726), ISSN: 1504-6109 (print), 1504-6192 (online), 2013.

Antón, M., Gil, J.E., Fernández-Gálvez, J., Lyamani, H., Valenzuela, A., Foyo-Moreno, I., Olmo, F. J., and Alados-Arboledas, L.: Evaluation of the aerosol forcing efficiency in the UV erythemal range at Granada, Spain, J. Geophys. Res., 116, D20214, doi:10.1029/2011JD016112, 2011.

Antón, M., Sorribas, M., Bennouna, Y., Vilaplana, J. M., Cachorro, V. E., Gröbner, J., and Alados-Arboledas, L.: Effects of an extreme desert dust event on the spectral ultraviolet irradiance at El Arenosillo (Spain), J. Geophys. Res., 117, D03205, doi:10.1029/2011JD016645, 2012a.

588 Antón, M., Valenzuela, A., Cazorla, A., Gil, J.E., Fernández-Gálvez, J., Lyamani, H., Foyo-
589   Moreno, I., Olmo, F.J., Alados-Arboledas, L.: Global and diffuse shortwave irradiance during a
590   strong desert dust episode at Granada (Spain), Atmos. Res., 118, 232–239,
591   doi:10.1016/j.atmosres.2012.07.007, 2012b.

592 Antón, M., Valenzuela, A., Mateos, D., Alados, I., Foyo-Moreno, I., Olmo, F.J., Alados-Arboledas,
593   L.: Lonwave aerosol radiative effects during an extreme desert dust event in Southeastern
594   Spain, Atmos. Res., doi: 10.1016/j.atmosres.2014.05.022, 2014.

595 Barja, B., and Antuña, J.C.: The effect of optically thin cirrus clouds on solar radiation in
596   Camagüey Cuba. Atmos. Chem. Phys., 11, 8625–8634, doi:10.5194/acp-11-8625-2011, 2011.

597 Barmpadimos, I., Keller, J., Oderbolz, D., Hueglin C., and Prèvôt, A.S.H.: One decade of parallel
598   fine ($PM_{2.5}$) and coarse (PM_{10}- $PM_{2.5}$) particulate matter measurements in Europe: trends and
599   variability, Atmos. Chem. Phys. 12, 3189-3203, doi: 10.5194/acp-12.3189-2012, 2012.

600 Bennouna, Y., Cachorro, V., Toledano, C., Berjón, A., Prats, N., Fuertes, D., Gonzalez, R.,
601   Rodrigo, R., Torres, B., and de Frutos, A.: Comparison of atmospheric aerosol climatologies
602   over southwestern Spain derived from AERONET and MODIS, Rem. Sen. Env. 115, 1272-
603   1284, 2011.

604 Bennouna, Y. S., Cachorro, V.E., Torres, B., Toledano, C., Berjón, A., de Frutos, A.M., and
605   Fernández-Coopel, A.: Atmospheric turbidity determined by the annual cycle of the aerosol
606   optical depth over north-center Spain from ground (AERONET) and satellite (MODIS), Atmos.
607   Environ., 67, 352–364, doi: 10.1016/j.atmosenv.2012.10.065, 2013.

608 Bennouna, Y.S., Cachorro, V., Burgos, M.A., Toledano, C., Torres, B., and de Frutos, A.:
609   Relationships between columnar aerosol optical properties and surface Particulate Matter

610   observations in north-central Spain from long-term records (2003-2011), Atmos. Meas. Tech.

611   Discuss., In press, 2014.

612 Bilbao, J., Román, R., de Miguel, A., and Mateos, D.: Long-term solar erythemal UV irradiance

613   data reconstruction in Spain using a semiempirical method, J. Geophys. Res., 116, D22211,

614   doi:10.1029/2011JD015836, 2011.

615 Bush, B. C., and Valero, F. P. J.: Surface aerosol radiative forcing at Gosan during the ACE– Asia

616   campaign, J. Geophys. Res., 108(D23), 8660, doi:10.1029/2002JD003233, 2003.

617 Cachorro, V.E., Vergaz, R., de Frutos, A.M., Vilaplana, J.M., Henriques, D., Laulainen, N., and

618   Toledano, C.: Study of desert dust events in the southwestern of the Iberian Peninsula in year

619   2000: two case studies, Annales Geophysicae 24, 1-18, 2006.

620 Cachorro, V. E., Toledano, C., Prats, N., Sorribas, M., Mogo, S., Berjón, A., Torres, B., Rodrigo,

621   R., de la Rosa, J., and De Frutos, A. M.: The strongest desert dust intrusion mixed with smoke

622   over the Iberian Peninsula registered with Sun photometry, J. Geophys. Res., 113, D14S04,

623   doi:10.1029/2007JD009582, 2008.

624 Collaud Coen, M., Andrews, E., Asmi, A., Baltensperger, U., Bukowiecki, N., Day, D., Fiebig, M.,

625   Fjaeraa, A. M., Flentje, H., Hyvärinen, A., Jefferson, A., Jennings, S. G., Kouvarakis, G.,

626   Lihavainen, H., Lund Myhre, C., Malm, W. C., Mihapopoulos, N., Molenar, J. V., O'Dowd, C.,

627   Ogren, J. A., Schichtel, B. A., Sheridan, P., Virkkula, A., Weingartner, E., Weller, R., and

628   Laj, P.: Aerosol decadal trends – Part 1: In-situ optical measurements at GAW and IMPROVE

629   stations, Atmos. Chem. Phys., 13, 869-894, doi:10.5194/acp-13-869-2013, 2013.

630 Córdoba-Jabonero, C., Sorribas, M., Guerrero-Rascado, J.L., Adame, J.A., Hernández, Y.,

631   Lyamani, H., Cachorro, V., Gil, M., Alados-Arboledas, L., Cuevas, E., and de la Morena, B.:

632   Synergetic monitoring of Saharan dust plumes and potential impact on surface: a case study of

27

633   dust transport from Canary Islands to Iberian Peninsula, Atmos. Chem. Phys., 11, 3067-3091,

634   doi:10.5194/acp-11-3067-2011, 2011.

635   Costa, M. J., Levizzani, V., and Silva, A. M.: Aerosol Characterization and Direct Radiative

636   Forcing Assessment over the Ocean. Part II: Application to Test Cases and Validation. J. Appl.

637   Meteor., 43, 1818–1833, doi: http://dx.doi.org/10.1175/JAM2157.1, 2004.

638   Costa, M.J., Sohn, B.J., Levizzani, V., and Silva, A.M.: Radiative forcing of Asian dust determined

639   from the synergized GOME and GMS satellite data - A case study, J. Meteorol. Soc. Jpn.,

640   84(1), 85-95, doi: 10.2151/jmsj.84.85, 2006.

641   Cusack, M., Alastuey, A., Pérez, N., Pey, J., and Querol, X.: Trends of particulate matter ($PM_{2.5}$)

642   and chemical composition at a regional site in the Western Mediterranean over the last nine

643   years (2002-2010), Atmos. Env. 12, 8341-8357, doi: 10.5194/acp-12-8341-2012, 2012.

644   de Miguel, A., Mateos, D., Bilbao, J., and Román, R.: Sensitivity analysis of ratio between

645   ultraviolet and total shortwave solar radiation to cloudiness, ozone, aerosols and precipitable

646   water, Atmos. Res., 102, 136–144, doi:10.1016/j.atmosres.2011.06.019., 2011.

647   Di Biagio, C., di Sarra, A., Meloni, D., Monteleone, F., Piacentino, S., and Sferlazzo, D.:

648   Measurements of Mediterranean aerosol radiative forcing and influence of the single scattering

649   albedo, J. Geophys. Res., 114, D06211, doi:10.1029/2008JD011037, 2009.

650   Di Biagio, C., di Sarra, A., and Meloni, D.: Large atmospheric shortwave radiative forcing by

651   Mediterranean aerosols derived from simultaneous ground-based and spaceborne observations

652   and dependence on the aerosol type and single scattering albedo, J. Geophys. Res., 115,

653   D10209, doi:10.1029/2009JD012697, 2010.

654   di Sarra, A., Pace, G, Meloni, D., De Silvestri, L., Piacentino, S., and Monteleone, F.: Surface

655   shortwave radiative forcing of different aerosol types in the Mediterranean, Geophys. Res.

656   Lett., 35, L02714, doi:10.1029/2007GL032395, 2008.

657   di Sarra, A., Di Biagio, C., Meloni, D., Monteleone, F., Pace, G., Pugnaghi, S., and Sferlazzo, D.:

658   Shortwave and longwave radiative effects of the intense Saharan dust event of 25–26 March

659   2010 at Lampedusa (Mediterranean Sea), J. Geophys. Res., 116, D23209,

660   doi:10.1029/2011JD016238, 2011.

661   Díaz, A. M., et al.: Aerosol radiative forcing efficiency in the UV region over southeastern

662   Mediterranean: VELETA2002 campaign, J. Geophys. Res., 112, D06213,

663   doi:10.1029/2006JD007348, 2007.

664   Dubovik, O., and King, M.D.: A flexible inversion algorithm for retrieval of aerosol optical

665   properties from Sun and sky radiance measurements, J. Geophys. Res., 105, 20673-20696,

666   2000.

667   Dubovik, O., Smirnov, A., Holben, B.N., King, M.D., Kaufman, Y.J., Eck, T.F., and Slutsker, I.:

668   Accuracy assessments of aerosol optical properties retrieved from Aerosol Robotic Network

669   (AERONET) Sun and sky radiance measurements, J. Geophys. Res., 105, 9791-9806, 2000.

670   Dubovik, O., et al.: Application of spheroid models to account for aerosol particle nonsphericity in

671   remote sensing of desert dust, J. Geophys. Res., 111, D11208, 2006.

672   Esteve, A.R., Estellés, V., Utrillas, M.P., and Martínez-Lozano, J.A.: Analysis of the aerosol

673   radiative forcing over a Mediterranean urban coastal site, Atmos. Res., 137, 194-204,

674   http://dx.doi.org/10.1016/j.atmosres.2013.10.009, 2014.

675   Forster, P., et al.: Changes in atmospheric constituents and in radiative forcing, in *Climate Change*

676   *2007: The Physical Science Basis. Contribution of Working Group I to the Fourth Assessment*

677   *Report of the Intergovernmental Panel on Climate Change*, edited by S. Solomon et al., 129-

678   234, Cambridge Univ. Press, Cambridge, U.K, 2007.

679   Foyo-Moreno, I., Alados, I., Antón, M., Fernández-Gálvez, J., Cazorla, A., and Alados-Arboledas,

680   L.: Estimating aerosol characteristics from solar irradiance measurements at an urban location

681   in Southeastern Spain, Journal of Geophysical Research: Atmospheres, In press, 2014.

682   García, O. E., Díaz, A. M., and Expósito, F. J.: Validation of AERONET estimates of atmospheric

683   solar fluxes and aerosol radiative forcing by ground-based broadband measurements, J.

684   Geophys. Res., 113, D21207, doi:10.1029/2008JD010211, 2008.

685   García, R.D., García, O.E., Cuevas, E., Cachorro, V.E., Romero-Campos, P.M., Ramos, R., and de

686   Frutos, A.M.: Solar radiation measurements compared to simulations at the BSRN Izaña

687   station: Mineral dust radiative forcing and efficiency study, J. Geophys. Res. Atmos., 119, 179–

688   194, doi:10.1002/2013JD020301, 2014.

689   Guerrero-Rascado, J.L., Ruiza, B., and Alados-Arboledas, L.: Multi-spectral Lidar characterization

690   of the vertical structure of Saharan dust aerosol over southern Spain, Atmos. Env., 42(11),

691   2668–2681, 2008.

692   Guerrero-Rascado, J.L., Olmo, F. J., Avilés-Rodríguez, I., Navas-Guzmán, F., Pérez-Ramírez, D.,

693   Lyamani, H., and Alados-Arboledas, L.: Extreme Saharan dust event over the southern Iberian

694   Peninsula in September 2007: active and passive remote sensing from surface and Satellite,

695   Atmos. Chem. Phys., 9, 8453–8469, doi:10.5194/acp-9-8453-2009, 2009.

696   Gueymard, C.: The sun's total and spectral irradiance for solar energy applications and solar

697   radiation models, Sol. Energy, 76, 423-453, 2004.

698   Hansen, J. E., Sato, M., Lacis, A., Ruedy, R., Tegen, I., and Matthews, E.: Climate forcings in the

699   industrial era, Proc. Natl. Acad. Sci. U.S.A., 95, 12753–12758, doi:10.1073/pnas.95.22.12753,

700   1998.

701   Hatzianastassiou, N., Katsoulis, B., and Vardavas, I.: Global distribution of aerosol direct radiative

702   forcing in the ultraviolet and visible arising under clear skies, Tellus B, 56, 51–71,

703   doi:10.1111/j.1600-0889.2004.00085.x, 2004.

704   Hess, M., Koepke, P., and Schult, I.: Optical Properties of Aerosols and Clouds: The Software

705   Package OPAC, Bull. Am. Meteorol. Soc., 79, 831-844, 1998.

706   Holben, B.N., et al.: AERONET – A federated instrument network and data archive for aerosol

707   characterization, Rem. Sen. Environ., 66, 1–16, 1998.

708   Horvath, H., Alados Arboledas, L., Olmo, F. J., Jovanovic, O., Gangl, M., Kaller, W., Sánchez, C.,

709   Sauerzopf, H., and Seidl, S.: Optical characteristics of the aerosol in Spain and Austria and its

710   effect on radiative forcing, J. Geophys. Res., 107(D19), 4386, doi:10.1029/2001JD001472,

711   2002.

712   Jayaraman, A., Lubin, D., Ramachandran, S., Ramanathan, V. , Woodbridge, E., Collins, W. D.,

713   and Zalpuri, K. S.: Direct observations of aerosol radiative forcing over the tropical Indian

714   Ocean during the Janauary–February 1996 pre-INDOEX cruise, J. Geophys. Res., 103, 13,827–

715   13,836, doi:10.1029/98JD00559, 1998.

716   Kazadzis, S., Kouremeti, N., Bais, A., Kazantzidis, A., and Meleti, C.: Aerosol forcing efficiency in

717   the UVA region from spectral solar irradiance measurements at an urban environment, Ann.

718   Geophys., 27, 2515–2522, doi:10.5194/angeo-27-2515-2009, 2009.

719   Lucht, W. and Roujean, J.L.: Consideration in parametric modelling of BRDF and albedo from

720   multi-angular satellite sensors observations, Remote Sens. Rev., 18, 343–379, 2000.

721 Lyamani, H., Olmo, F.J., and Alados-Arboledas, L.: Saharan dust outbreak over southeastern Spain

722   as   detected   by   sun   photometer,   Atmos.   Env.,   39,   7276-7284,

723   doi:10.1016/j.atmosenv.2005.09.011, 2005.

724 Lyamani, H., Olmo, F. J., Alcántara, A., and Alados-Arboledas, L.: Atmospheric aerosols during

725   the 2003 heat wave in southeastern Spain II: Microphysical columnar properties and radiative

726   forcing, Atmos. Environ., 40, 6465–6476, doi:10.1016/j.atmosenv.2006.04.047, 2006.

727 Lyamani, H., Fernández-Gálvez, J., Pérez-Ramírez, D., Valenzuela, A., Antón, M., Alados, I.,

728   Titos, G., Olmo, F.J., and Alados-Arboledas, L.: Aerosol properties over two urban sites in

729   South Spain during an extended stagnation episode in winter season, Atmos. Env. 62, 424-432,

730   2012.

731 Mallet, M., Dubovik, O., Nabat, P., Dulac, F., Kahn, R., Sciare, J., Paronis, D., and Leon, J.F.:

732   Absorption properties of Mediterranean aerosols obtained from multi-year ground-based

733   remote sensing observations, Atmos. Chem. Phys., 13, 9195-9210, doi:10.5194/acp-13-9195-

734   2013, 2013.

735 Mateos, D., Bilbao, J., de Miguel, A., and Pérez-Burgos, A.: Dependence of ultraviolet (erythemal

736   and total) radiation and CMF values on total and low cloud covers in Central Spain, Atmos.

737   Res., 98, 21-27, doi:10.1016/j.atmosres.2010.05.002, 2010.

738 Mateos, D., Antón, M., Sanchez-Lorenzo, A., Calbó, J., and Wild, M.: Long-term changes in the

739   radiative effects of aerosols and clouds in a mid-latitude region (1985–2010), Global Planet.

740   Change, 111, 288-295, http://dx.doi.org/10.1016/j.gloplacha.2013.10.004, 2013a.

741 Mateos, D., Antón, M., Valenzuela, A., Cazorla, A., Olmo, F.J., and Alados-Arboledas, L.: Short-

742   wave radiative forcing at the surface for cloudy systems at a midlatitude site, Tellus B, 65,

743   21069, http://dx.doi.org/10.3402/tellusb.v65i0.21069, 2013b.

744   Mateos, D., Pace, G., Meloni, D., Bilbao, J., di Sarra, A., Casasanta, G., de Miguel, A., and Min,

745   Q.: Observed influence of liquid cloud microphysical properties on ultraviolet surface

746   radiation, J. Geophys. Res., 119, doi:10.1002/2013JD020309, 2014.

747   Mayer, B., and Kylling, A.: Technical note: The libRadtran software package for radiative transfer

748   calculations – description and examples of use, Atmos. Chem.Phys., 5, 1855–1877, 2005.

749   Meloni, D., di Sarra, A., DeLuisi, J., Di Iorio, T., Fiocco, G., Junkerman, W., and Pace, G.:

750   Tropospheric aerosols in the Mediterranean: 2. Radiative effects through model simulations and

751   measurements, J. Geophys. Res., 108(D10), 4317, doi:10.1029/2002JD002807, 2003.

752   Meloni, D., di Sarra, A., Di Iorio, T., and Fiocco, G.: Influence of the vertical profile of Saharan

753   dust on the visible direct radiative forcing, J. Quant. Spectrosc. Radiat. Transfer, 93, 397–413,

754   2005.

755   Moody, E.G., King, M.D., Platnick, S., Schaaf, C.B., and Gao, F.: Spatially complete global

756   spectral surface albedos: value-added datasets derived from Terra MODIS land products, IEEE

757   T. Geosci. Remote., 43, 144–158, 2005.

758   Navas-Guzmán, F., Bravo-Aranda, J.A., Guerrero-Rascado, J.L., Granados-Muñoz, M.J., and

759   Alados-Arboledas, L.: Statistical analysis of aerosol optical properties retrieved by Raman lidar

760   over Southeastern Spain, Tellus B, 65, 21234, http://dx.doi.org/10.3402/tellusb.v65i0.21234,

761   2013.

762   Nikitidou, E., Kazantzidis, A., De Bock, V., and De Backer, H.: The aerosol forcing efficiency in

763   the UV region and the estimation of single scattering albedo at a typical West European site,

764   Atmos. Env., 69, 313-320, doi:http://dx.doi.org/10.1016/j.atmosenv.2012.12.035, 2013.

765 Obregón M.A., Pereira S, Wagner F, Serrano A, Cancillo ML, Silva AM.: Regional differences of

766   column aerosol parameters in western Iberian Península, Atmos. Environ., 62, 208-219, doi:

767   10.1016/j.atmosenv.2012.08.016, 2012

768 Pace, G., di Sarra, A., Meloni, D., Piacentino, S., and Chamard, P.: Aerosol optical properties at

769   Lampedusa (central Mediterranean): 1. Influence of transport and identification of different

770   aerosol types, Atmos. Chem. Phys., 6, 697‑713, 2006.

771 Panicker, A. S., Pandithurai, G., Safai, P. D., and Kewat, S.: Observations of enhanced aerosol

772   longwave radiative forcing over an urban environment, Geophys. Res. Lett., 35, L04817,

773   doi:10.1029/2007GL032879, 2008.

774 Penner, J. E., et al.: Aerosols, their Direct and Indirect Effects, in *Climate Change 2001: The*

775   *Scientific Basis*, edited by: Houghton, J. T., Ding, Y., Griggs, D. J., Noguer, M., Van der

776   Linden, P. J., Dai, X., Maskell, K., and Johnson, C. A., Report to Intergovernmental Panel on

777   Climate Change from the Scientific Assessment Working Group (WGI), Cambridge University

778   Press, 289–416, 2001.

779 Pérez-Ramírez, D., Aceituno, J., Ruiz, B., Olmo, F.J., and Alados-Arboledas, L.: Development and

780   calibration of a star photometer to measure the aerosol optical depth: Smoke observations at a

781   high mountain site, Atmos. Env. 42(11), 2733–2738, 2008.

782 Pey, J., Querol, X, Alastuey, A., Forastiere, F, and Stafoggia, M. African dust outbreaks over the

783   Mediterranean Basin during 2001–2011: PM_{10} concentrations, phenomenology and trends, and

784   its relation with synoptic and mesoscale meteorology, Atmos. Chem. Phys., 13, 1395-1410,

785   doi:10.5194/acp-13-1395-2013, 2013.

786   Prats, N., Cachorro, V.E., Berjón, A., Toledano, C., and De Frutos, A.M.: Column-integrated

787   aerosol microphysical properties from AERONET Sun photometer over south-western Spain.

788   Atmos. Chem. Phys. 11, 12353-12547, doi:10.5194/acpd-11-12353-2011, 2011.

789   Querol, X., Alastuey, A., Pandolfi, M., Reche, C., Pérez, N., Minguillón, M.C., Moreno, T., Viana,

790   M., Escudero, M., Orio, A., Pallarés, M., and Reina, F.: 2001-2012 trends of air quality in

791   Spain, Sci. Total Environ., 490, 957-969.

792   Rajeev, K., and Ramanathan, V.: Direct observations of clear-sky aerosol radiative forcing from

793   space during the Indian Ocean Experiment, J. Geophys. Res., 106, 17,221–17,235,

794   doi:10.1029/2000JD900723, 2001.

795   Reche, C., et al.: Peculiarities in atmospheric particle number and size-resolved speciation in an

796   urban area in the western Mediterranean: Results from the DAURE campaign, Atmos. Env., 45,

797   5282-5293, doi:10.1016/j.atmosenv.2011.06.059, 2011.

798   Román, R., Antón, M., Valenzuela, A., Gil, J.E., Lyamani, H., de Miguel, A., Olmo, F.J., Bilbao, J.,

799   and Alados-Arboledas, L.: Evaluation of the desert dust effects on global, direct, and diffuse

800   spectral ultraviolet irradiance, Tellus B, 65, 19578,

801   http://dx.doi.org/10.3402/tellusb.v65i0.19578, 2013.

802   Román, R., Bilbao, J., and de Miguel, A.: Solar radiation simulations in the Iberian Peninsula:

803   Accuracy and sensitivity to uncertainties in inputs of a radiative transfer model, J. Quant.

804   Spectrosc. Ra., 145, 95-109, 2014.

805   Ruckstuhl, C., et al.: Aerosol and cloud effects on solar brightening and the recent rapid warming,

806   Geophys. Res. Lett., 35, L12708, doi:10.1029/2008GL034228, 2008.

Saha, A., Mallet, M., Roger, J. C., Dubuisson, P., Piazzola, J., and Despiau, S.: One year measurements of aerosol optical properties over an urban coastal site: Effect on local direct radiative forcing, Atmos. Res., 90, 195–202, doi:10.1016/j.atmosres.2008.02.003, 2008.

Sanchez-Lorenzo, A., Calbó, J., and Wild, M.: Global and diffuse solar radiation in Spain: Building a homogeneous dataset and assessing trends, Global Planet. Change, 100, 343-352, http://dx.doi.org/10.1016/j.gloplacha.2012.11.010, 2013.

Santos, D., Costa, M. J., and Silva, A. M.: Direct SW aerosol radiative forcing over Portugal, Atmos. Chem. Phys., 8, 5771–5786, doi:10.5194/acp-8-5771-2008, 2008.

Schuster, G. L., Dubovik, O., and Holben, B. N.: Angstrom exponent and bimodal aerosol size distributions, J. Geophys. Res., 111, D07207, doi:10.1029/2005JD006328, 2006.

Sen, P. K.: Estimates of the regression coefficient based on Kendall's tau, J. Am., Stat. Assoc., 63, 1379–1389, 1968.

Shettle, E. P.: Models of aerosols, clouds and precipitation for atmospheric propagation studies, paper presented at Conference on Atmospheric Propagation in the UV, Visible, IR and MM-Region and Related System Aspects, NATO Adv. Group for Aerosp. Res. and Dev., Copenhagen, 1989.

Stamnes, K., Tsay, S.C., Wiscombe, W., and Laszlo, I.: DISORT, a General-Purpose Fortran Program for Discrete-Ordinate-Method Radiative Transfer in Scattering and Emitting Layered Media: Documentation of Methodology, Tech. rep. Dept. of Physics and Engineering Physics, Stevens Institute of Technology, Hoboken, NJ 07030, 2000.

Steinbrecht, W., Köhler, U., Claude, H., Weber, M., Burrows, J.P., and van der A, R.J.: Very high ozone columns at northern mid-latitudes in 2010, Geophys Res Lett, 38, L06803, doi:10.1029/2010GL046634, 2011.

830   Toledano, C., Cachorro, V.E., Berjon, A., de Frutos, A.M., Sorribas, M., de la Morena, B., and

831   Goloub, P.: Aerosol optical depth and Ångström exponent climatology at El Arenosillo

832   AERONET site (Huelva, Spain), Q. J. R. Meterol. Soc., 133, 795-807, 2007a.

833   Toledano, C., Cachorro, V.E., de Frutos, A.M., Sorribas, M., Prats, N., and de la Morena, B.:

834   Inventory of African desert dust events over the southwestern Iberian Peninsula in 2000-2005

835   with an AERONET Cimel Sun photometer, J. Geophys. Res. 112, doi:10.1029/2006JD008307,

836   2007b.

837   Valenzuela, A., Olmo, F.J., Lyamani, H., Antón, M., Quirantes, A., and Alados-Arboledas, L.:

838   Aerosol radiative forcing during African desert dust events (2005-2010) over Southeastern

839   Spain, Atmos. Chem. Phys. 12, 10331–10351, doi:10.5194/acp-12-10331-2012, 2012.

840   Zhou, M., Yu, H., Dickinson, R. E., Dubovik, O., and Holben, B. N.: A normalized description of

841   the direct effect of key aerosol types on solar radiation as estimated from Aerosol Robotic

842   Network aerosols and Moderate Resolution Imaging Spectroradiometer albedos, J. Geophys.

843   Res., 110, D19202, doi:10.1029/2005JD005909, 2005.

844

845 Tables

846
847 **Table 1.** Coordinates and time interval of the six AERONET sites used in this study.

Station	Latitude (ºN)	Longitude (ºE)	Altitude a.s.l. (m)	Time interval
Palencia	41.99	-4.52	750	2003-2012
Barcelona	41.39	2.12	125	2004-2012
Cabo da Roca	38.78	-9.50	140	2003-2011
Évora	38.57	-7.91	293	2005-2012
Granada	37.16	-3.61	680	2004-2012
El Arenosillo	37.11	-6.73	0	2000-2009

848
849
850
851
852 **Table 2.** Summary of AERONET data used for ARE calculations: aerosol optical depth (AOD),
853 single scattering albedo (SSA), asymmetry factor (g), precipitable water vapor column (PWC).
854 Estimated absolute uncertainty of AOD and SSA is given according to Dubovik et al. (2002), and
855 PWC error from Holben et al. (1998).

	AERONET database	Estimated uncertainty
AOD	Level 2.0	±0.01-0.02
SSA, g ($AOD_{440}>0.4$)	Level 2.0	±0.03 (in SSA)
SSA, g ($0.15<AOD_{440}<0.4$)	Level 1.5-filtered*	±0.05-0.07 (in SSA)
SSA, g ($AOD_{440}<0.15$)	Fixed value	
PWC	Level 2.0	10-15%

856 *Filters applied are the same as in level 2.0 except for AOD_{440} (see text).

857
858
859
860
861 **Table 3.** AFE values and their standard error for the UV, VIS, NIR, and SW ranges for, separately,
862 four SSA and three α intervals over the Iberian Peninsula. Units are $Wm^{-2}\tau^{-1}$. SSA groups: $0.85 \geq$
863 $SSA_1 > 0.80$ (group 1), $0.90 \geq SSA_2 > 0.85$ (group 2), $0.95 \geq SSA_3 > 0.90$ (group 3), and $1.0 \geq$
864 $SSA_4 > 0.95$ (group 4); and α groups: $0 \leq \alpha_1 \leq 1$ (group 1), $1.0 \leq \alpha_2 \leq 1.5$ (group 2), and $1.5 < \alpha_3 \leq 2$
865 (group 3). The average values without any classification are also presented.
866

Variable	Group	AFE_{UV}	AFE_{VIS}	AFE_{NIR}	AFE_{SW}
α	1	-5.41 ± 0.06	-30.1 ± 0.3	-20.9 ± 0.2	-56.5 ± 0.5
	2	-6.60 ± 0.09	-38.3 ± 0.4	-19.1 ± 0.2	-64.0 ± 0.6
	3	-7.06 ± 0.10	-39.4 ± 0.4	-16.9 ± 0.2	-63.3 ± 0.7
SSA	1	-9.7 ± 0.2	-52.8 ± 0.8	-24.9 ± 0.5	-87.4 ± 1.4
	2	-8.19 ± 0.10	-44.6 ± 0.4	-21.2 ± 0.2	-74.0 ± 0.6
	3	-6.37 ± 0.05	-35.9 ± 0.2	-19.5 ± 0.2	-61.8 ± 0.3
	4	-4.59 ± 0.05	-26.6 ± 0.2	-18.1 ± 0.2	-49.3 ± 0.3
Average		-5.98 ± 0.05	-33.7 ± 0.2	-19.34 ± 0.11	-59.1 ± 0.3

867
868

Table 4. Daily Forcing Efficiencies at the surface by previous studies. Legend: desert dust (DD), continental-biomass burning (C-BB), and forest fires (FF).

Reference	Aerosol Type	AFE$_X$	Value (Wm^{-2}τ^{-1})	Time period	Region	More info.
Díaz et al. (2007)	Mixed	AFE$_{UV}$	-3	July 2002	Spain	290-363 nm
Meloni et al. (2005)	DD Mixed	AFE$_{VIS}$	-28.4 -45.6	July 2002	Central Mediterranean	
Lyamani et al. (2006)	Mixed	AFE$_{VIS}$	-75.8	August 2003	Spain	2003 heat wave
Di Biagio et al. (2010)	DD C-BB Mixed	AFE$_{SW}$	-68.9 -59.0 -94.9	2004-2007	Central Mediterranean	At the equinox
Esteve et al. (2014)	Mixed	AFE$_{SW}$	-139.0	2003-2011	Spain	200 cloud-free days
Santos et al. (2008)	FF	AFE$_{SW}$	-113.0	2004-2005	Portugal	Absorbing aerosols
di Sarra et al. (2011)	DD	AFE$_{SW}$	-55	25-26/03/2010	Central Mediterranean	Strong event
García et al. (2014)	DD	AFE$_{SW}$	-59	2009-2012	Canary Islands	386 cloud-free days
Costa et al. (2006)	DD	AFE$_{SW}$	-116.9	7/04/2000	Korea	SSA = 0.76
Zhou et al. (2005)	DD	AFE$_{SW}$	-80/-48	Monthly aerosol climatology	North Africa and Arabian Peninsula	Depending on surface albedo
Saha et al. (2008)	C-BB Mixed	AFE$_{SW}$	-97.6 -81.5	2005-2006	French Mediterranean	0.7 < SSA < 0.8
Valenzuela et al. (2012)	DD	AFE$_{SW}$	-70	2005-2010	Spain	

Table A1. Relative difference (RD) in the UV, VIS, NIR, and SW net fluxes between the case of SSA$_1$=0.8 and SSA$_2$=1.0 for different g and SZA values.

SZA	g	RD$_{UV}$ (%)	RD$_{VIS}$ (%)	RD$_{NIR}$ (%)	RD$_{SW}$ (%)
30°	0.65	-6.5	-3.7	-1.8	-3.0
	0.7	-6.5	-3.7	-1.8	-3.0
	0.75	-6.6	-3.8	-1.9	-3.1
	0.8	-6.7	-3.8	-1.9	-3.1
60°	0.65	-9.3	-5.7	-2.8	-4.5
	0.7	-9.4	-5.8	-2.9	-4.6
	0.75	-9.5	-5.9	-3.0	-4.7
	0.8	-9.6	-6.0	-3.0	-4.8

Figure Captions

Figure 1. Annual cycle of daily values of AOD at 440 nm by box whisker plots. Triangles and horizontal solid lines indicate the monthly average and median values, respectively.

Figure 2. Annual cycle of daily values of α ('alpha' in the figure) by box whisker plots. Triangles and horizontal solid lines indicate the monthly average and median values, respectively.

Figure 3. Relative frequency of aerosol type occurrence: maritime (MA), desert dust (DD), continental clean (CC), and continental polluted (CP).

Figure 4. Yearly values of AOD_{440nm} at the six sites: Barcelona (blue diamonds), Palencia (purple triangles), Évora (red squares), Cabo da Roca (grey crosses), Granada (black stars), and El Arenosillo (green circles). The text points out the statistically significant trend obtained.

Figure 5. Evolution of yearly ARE_{UV} (a), ARE_{VIS} (b), ARE_{NIR} (c), and ARE_{SW} (d) at the six sites: Barcelona (blue diamonds), Palencia (purple triangles), Évora (red squares), Cabo da Roca (grey crosses), Granada (black stars), and El Arenosillo (green circles). Vertical bars indicate the standard deviation of each yearly value at Palencia station.

Figure 6. Evolution of annual ARE at the four spectral ranges (ARE_{UV} purple diamonds, ARE_{VIS} red squares, ARE_{NIR} green triangles, and ARE_{SW} black circles) and AOD at 500 nm (blue stars) averaging the data from the six Iberian ground-based sites (only years with at least three sites considered). Dashed lines point out the linear trends (see text).
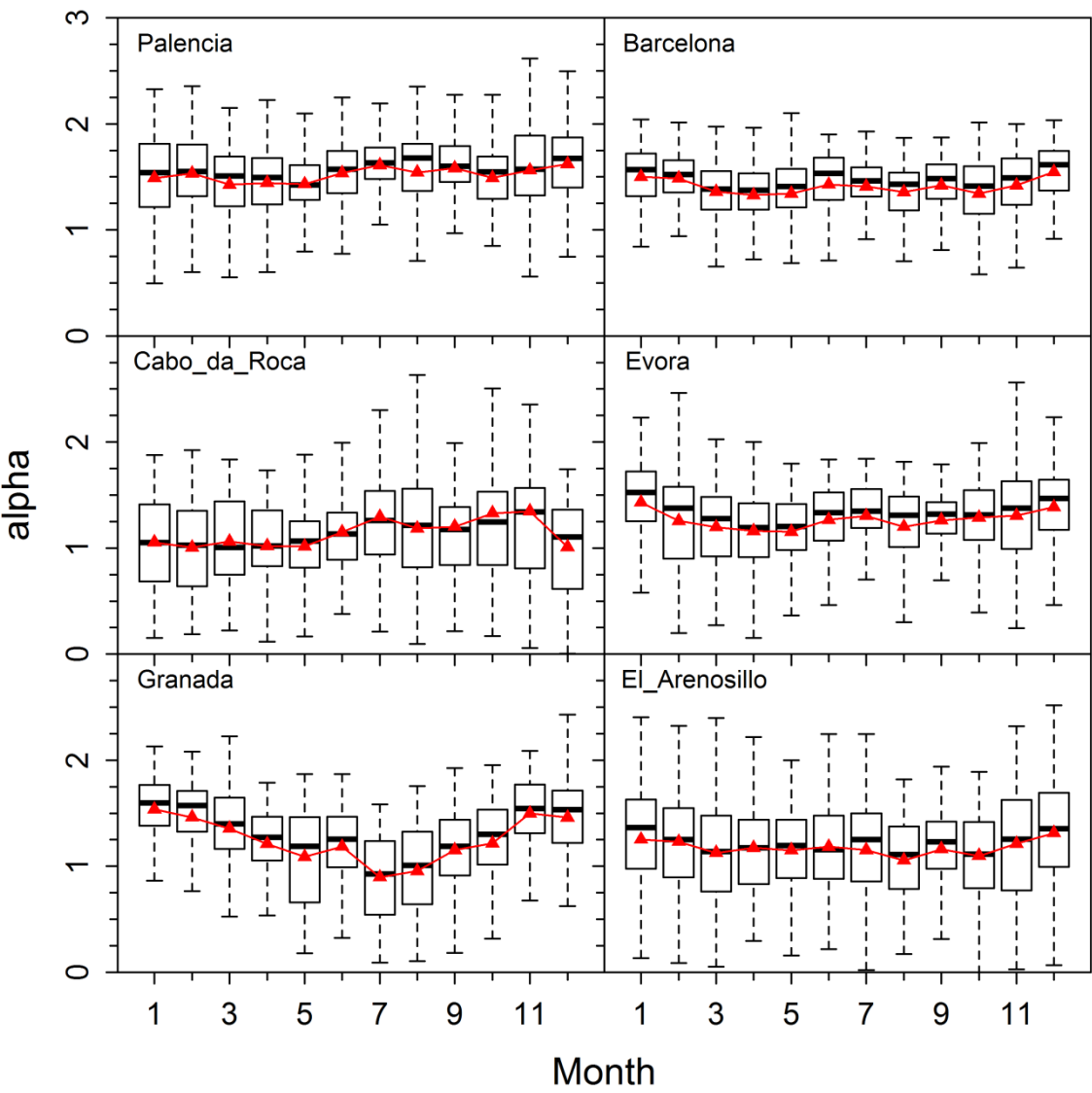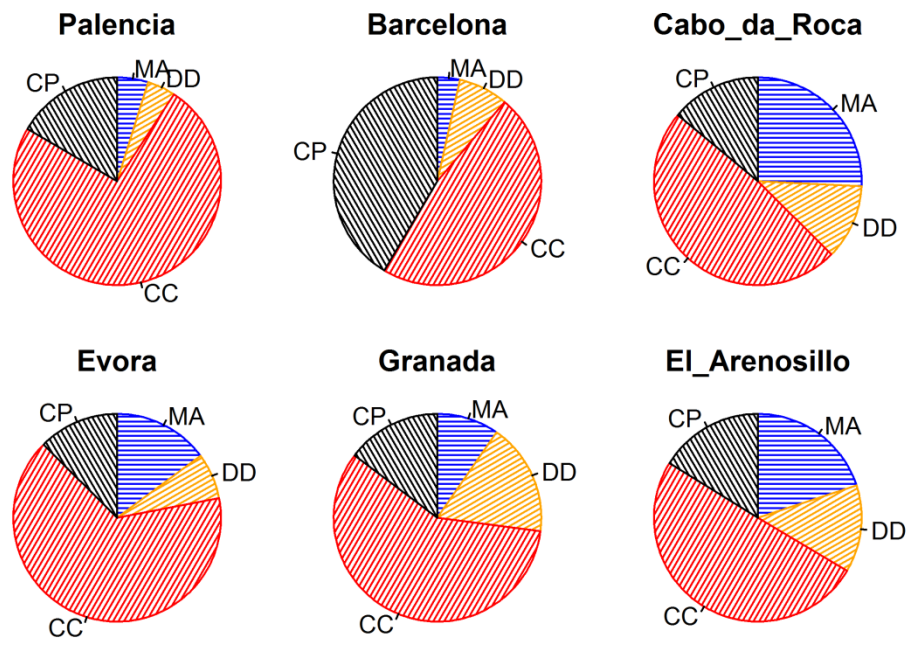
Figure 7. Annual cycle of ARE_{UV} (a), ARE_{VIS} (b), ARE_{NIR} (c), and ARE_{SW} (d) at the six sites: Barcelona (blue diamonds), Palencia (purple triangles), Évora (red squares), Cabo da Roca (grey crosses), Granada (black stars), and El Arenosillo (green circles). Vertical bars point out the standard deviation of each monthly value at Évora station.

902 **Figure 8.** AFE_{UV}, AFE_{VIS}, AFE_{NIR}, and AFE_{SW} against four groups of aerosol single scattering

903 albedo and three intervals of α at the six sites: Barcelona (blue diamonds), Palencia (purple

904 triangles), Évora (red squares), Cabo da Roca (grey crosses), Granada (black stars), and El

905 Arenosillo (green circles).

906 **Figure 9.** Dependence of AFE_{VIS}/AFE_{SW} (a, c, e) and AFE_{NIR}/AFE_{SW} (b, d, f) ratios on SSA for

907 large (a, b), medium (c, d) and small (e, f) particles at the six sites: Barcelona (blue diamonds),

908 Palencia (purple triangles), Évora (red squares), Cabo da Roca (grey crosses), Granada (black stars),

909 and El Arenosillo (green circles).

910

911   Figure 1
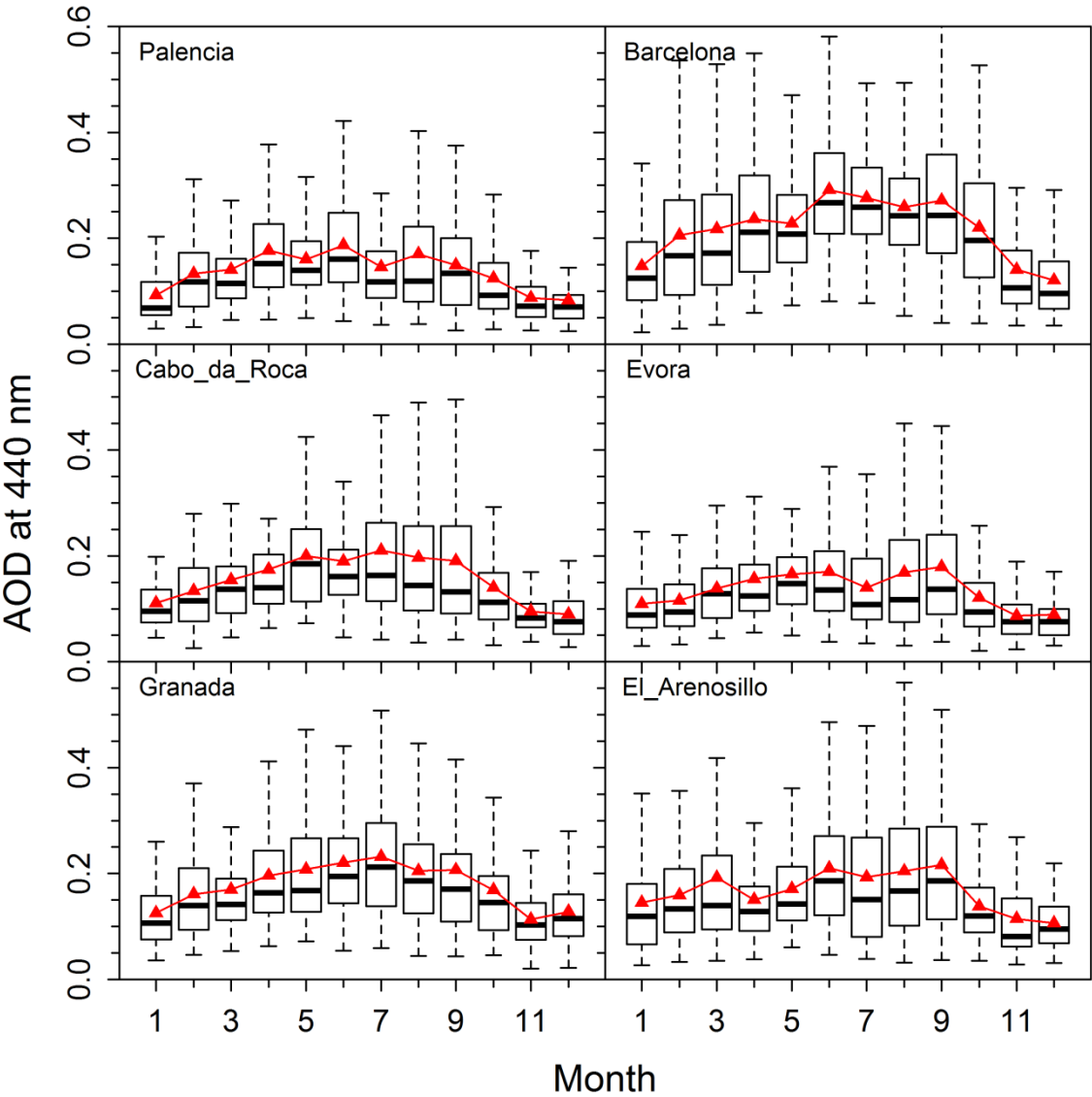
912

Figure 1. Annual cycle of daily values of AOD at 440 nm by box whisker plots. Triangles and

horizontal solid lines indicate the monthly average and median values, respectively.

915

916   Figure 2

918   **Figure 2.** Annual cycle of daily values of α ('alpha' in the figure) by box whisker plots. Triangles

919   and horizontal solid lines indicate the monthly average and median values, respectively.

920

921

922   Figure 3

923

Figure 3. Relative frequency of aerosol type occurrence: maritime (MA), desert dust (DD), continental clean (CC), and continental polluted (CP).

927

928   Figure 4

929
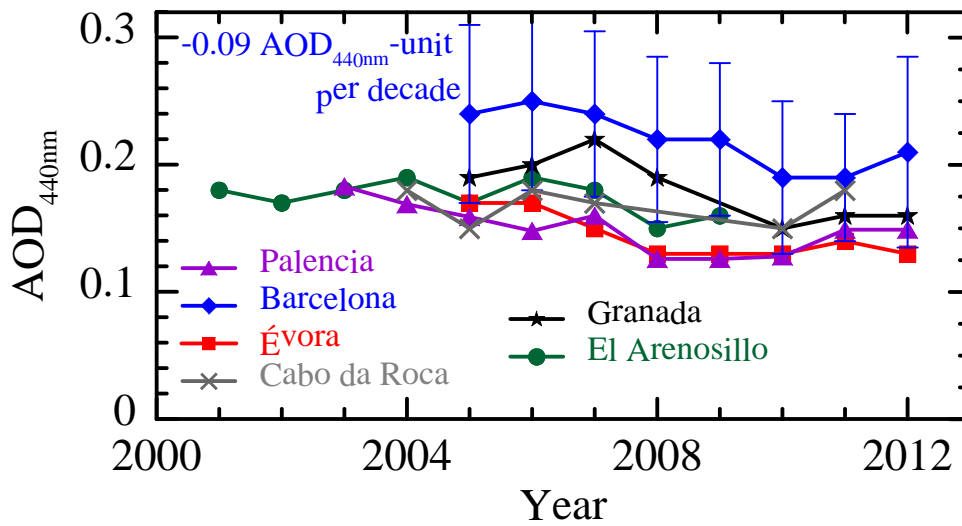
930

Figure 4. Yearly values of AOD_{440nm} at the six sites: Barcelona (blue diamonds), Palencia (purple triangles), Évora (red squares), Cabo da Roca (grey crosses), Granada (black stars), and El Arenosillo (green circles). The text points out the statistically significant trend obtained. Vertical bars indicate the standard deviation of each yearly value at Barcelona station.

935
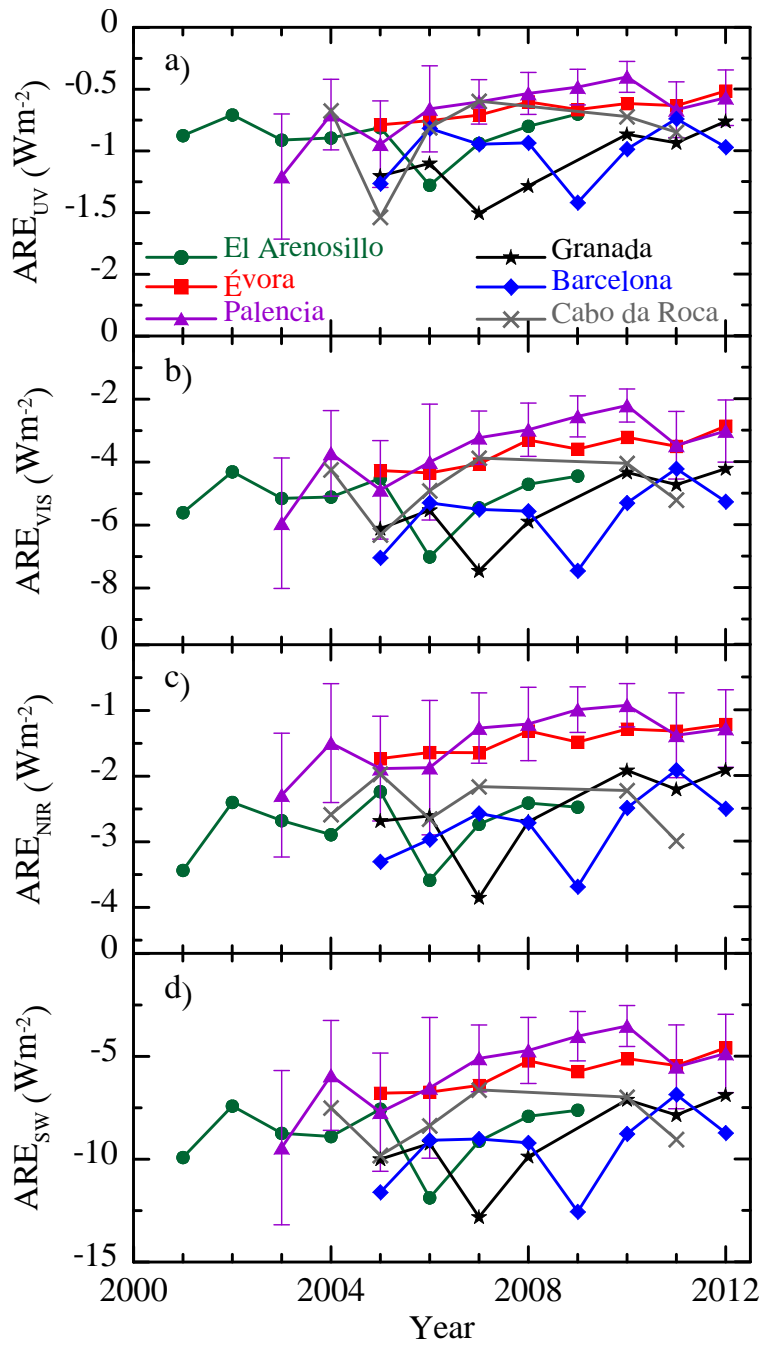
936   Figure 5

Figure 5. Evolution of yearly ARE_{UV} (a), ARE_{VIS} (b), ARE_{NIR} (c), and ARE_{SW} (d) at the six sites:
Barcelona (blue diamonds), Palencia (purple triangles), Évora (red squares), Cabo da Roca (grey
crosses), Granada (black stars), and El Arenosillo (green circles). Vertical bars indicate the standard
deviation of each yearly value at Palencia station.

942 Figure 6
943
944
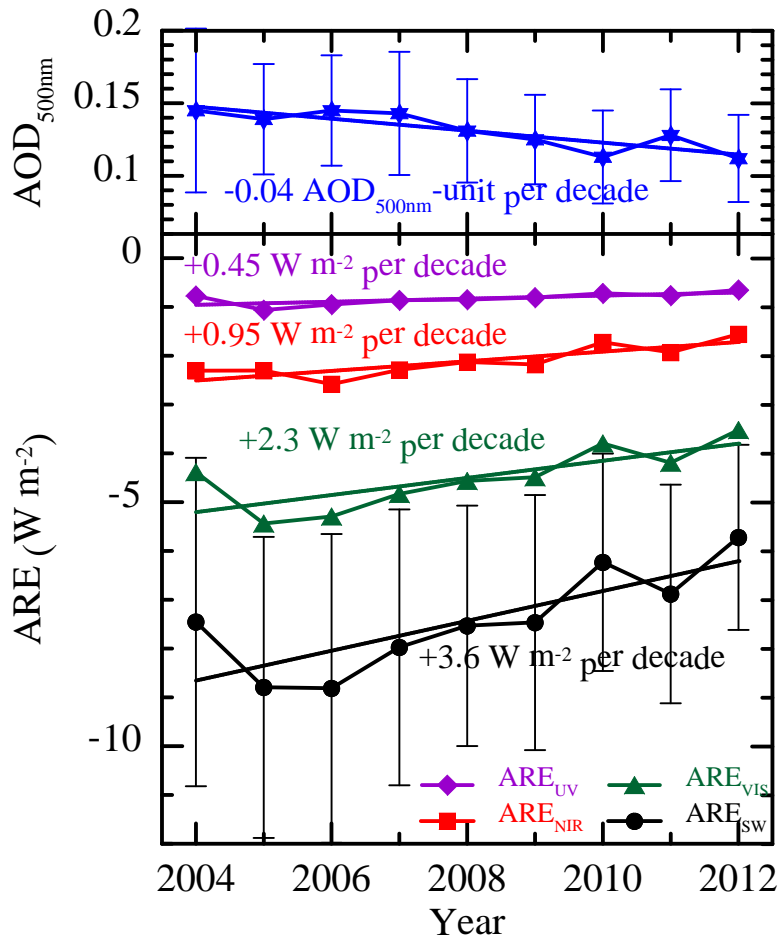
945
946

947 **Figure 6.** Evolution of annual ARE at the four spectral ranges (ARE$_{UV}$ purple diamonds, ARE$_{VIS}$

948 red squares, ARE$_{NIR}$ green triangles, and ARE$_{SW}$ black circles) and AOD at 500 nm (blue stars)

949 averaging the data from the six Iberian ground-based sites (only years with, at least, three sites are

950 considered). Dashed lines point out the linear trends (see text). Vertical bars indicate the standard
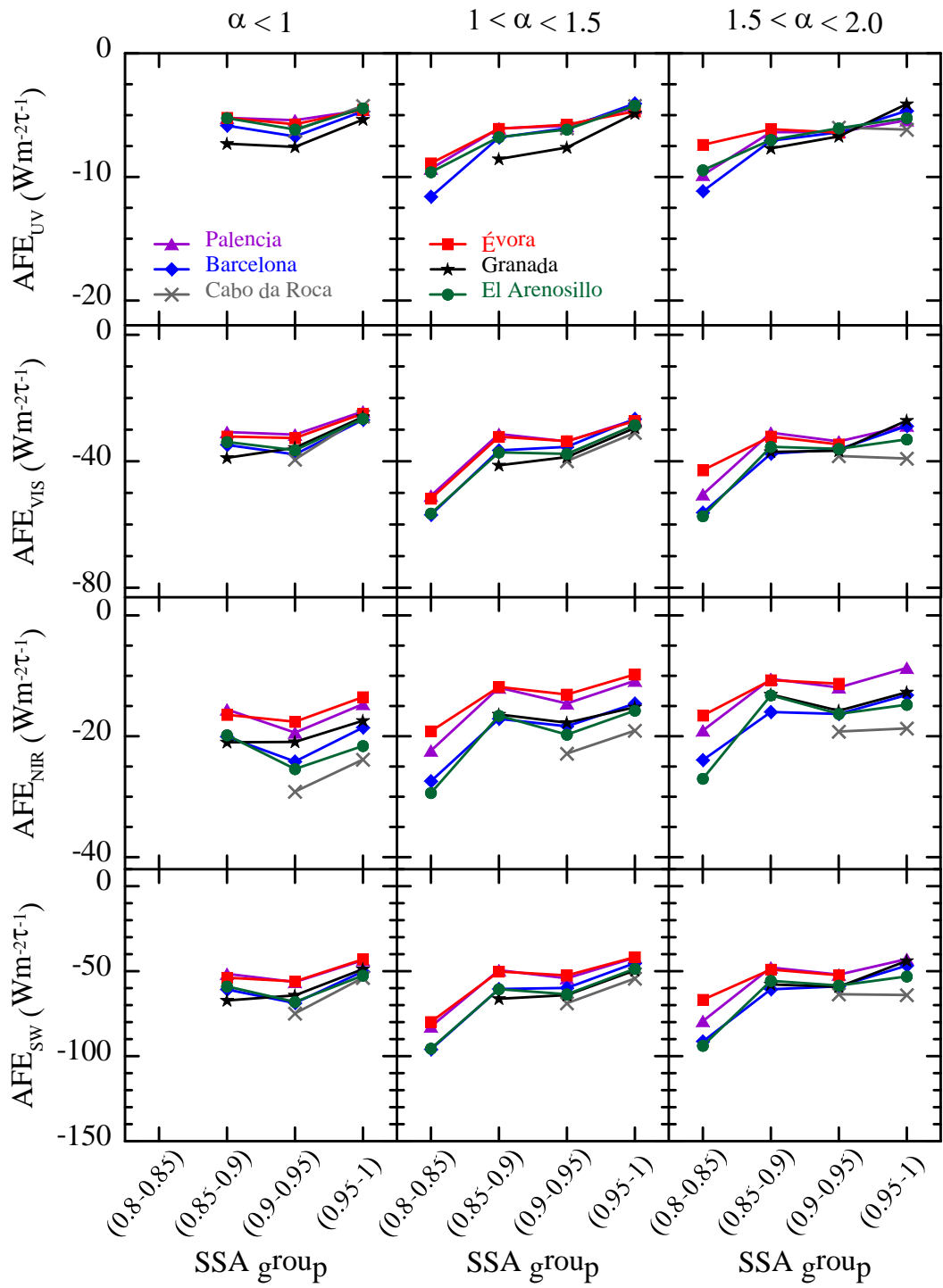
951 deviation.

952

953 Figure 7
954
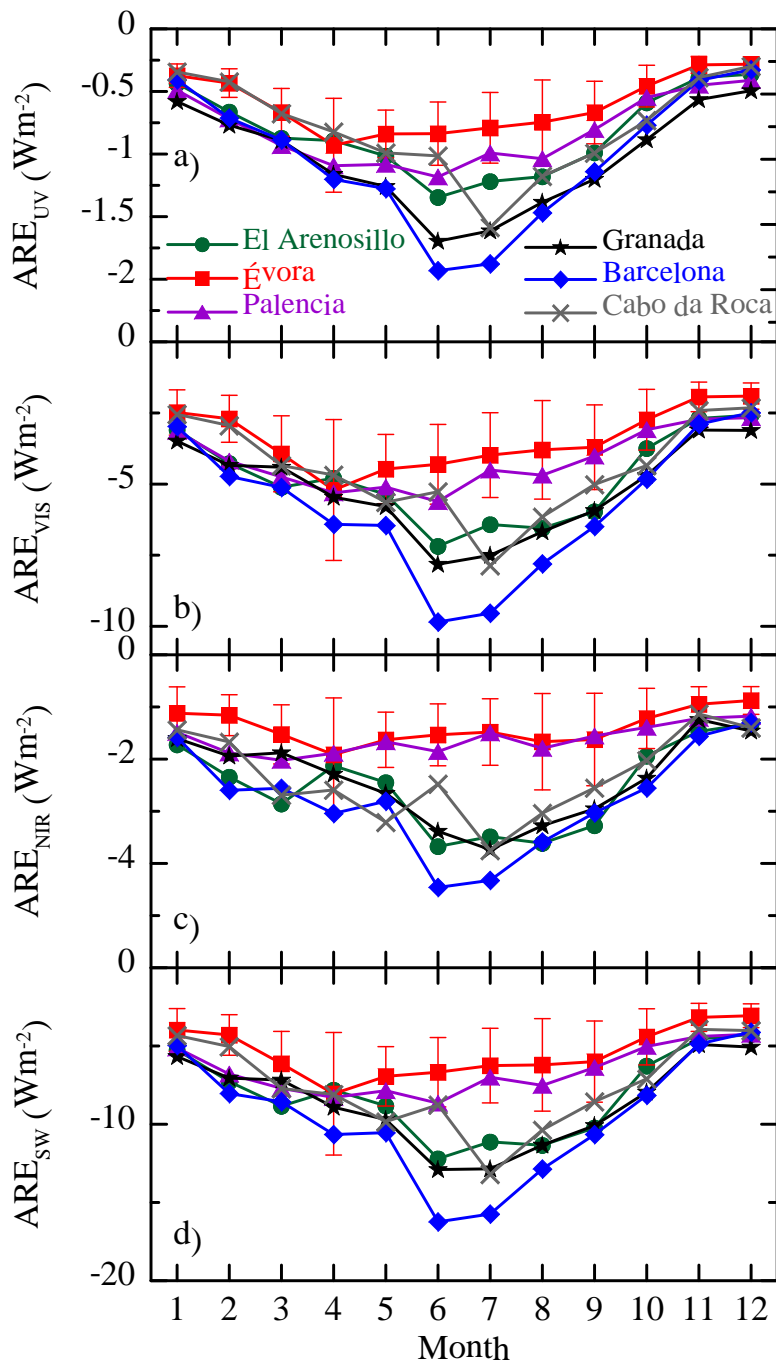
Figure 7. Annual cycle of ARE_{UV} (a), ARE_{VIS} (b), ARE_{NIR} (c), and ARE_{SW} (d) at the six sites: Barcelona (blue diamonds), Palencia (purple triangles), Évora (red squares), Cabo da Roca (grey crosses), Granada (black stars), and El Arenosillo (green circles). Vertical bars point out the standard deviation of each monthly value at Évora station.
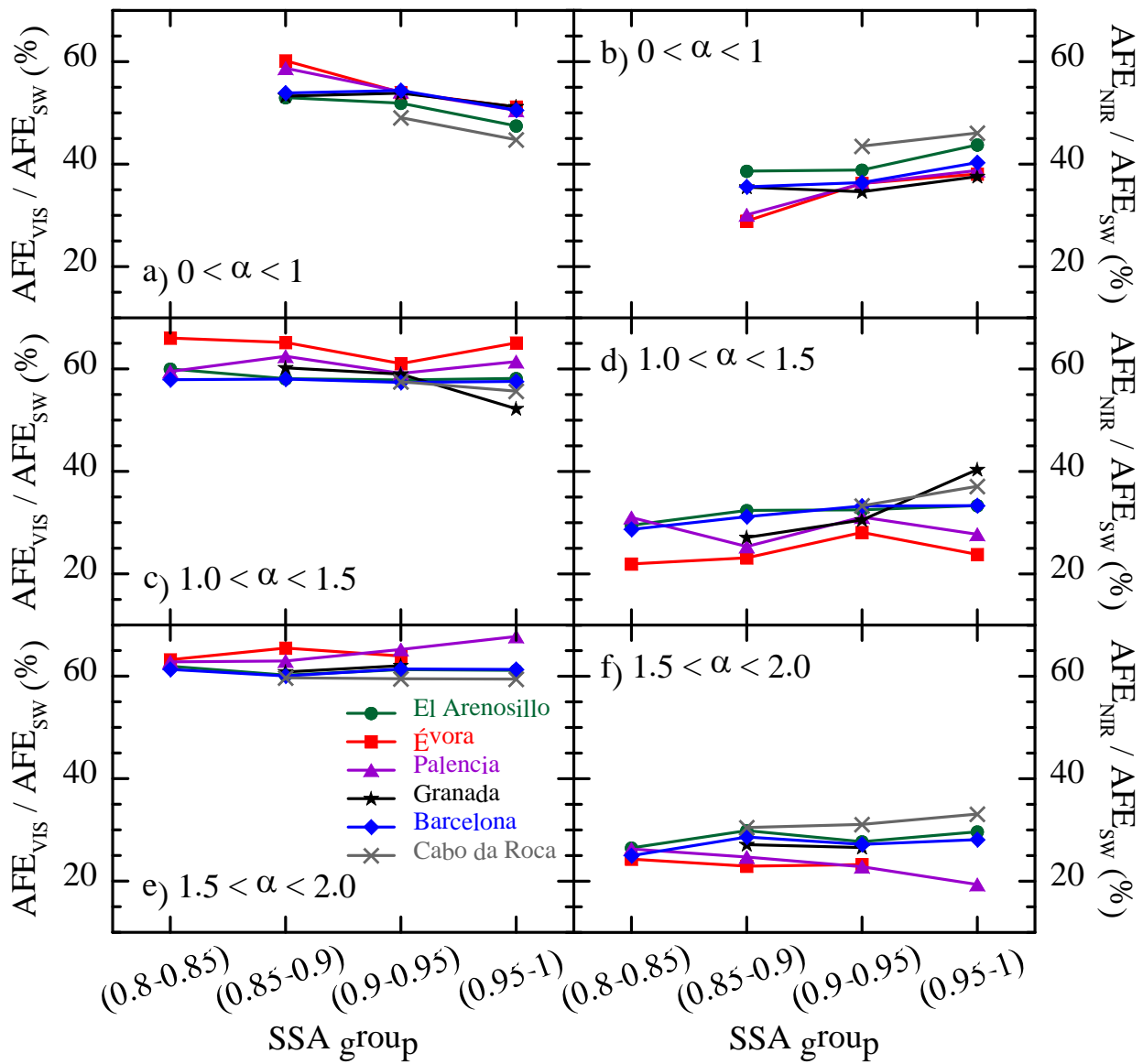
960   Figure 8

Figure 8. AFE_{UV}, AFE_{VIS}, AFE_{NIR}, and AFE_{SW} against four groups of aerosol single scattering albedo and three intervals of α at the six sites: Barcelona (blue diamonds), Palencia (purple triangles), Évora (red squares), Cabo da Roca (grey crosses), Granada (black stars), and El Arenosillo (green circles).

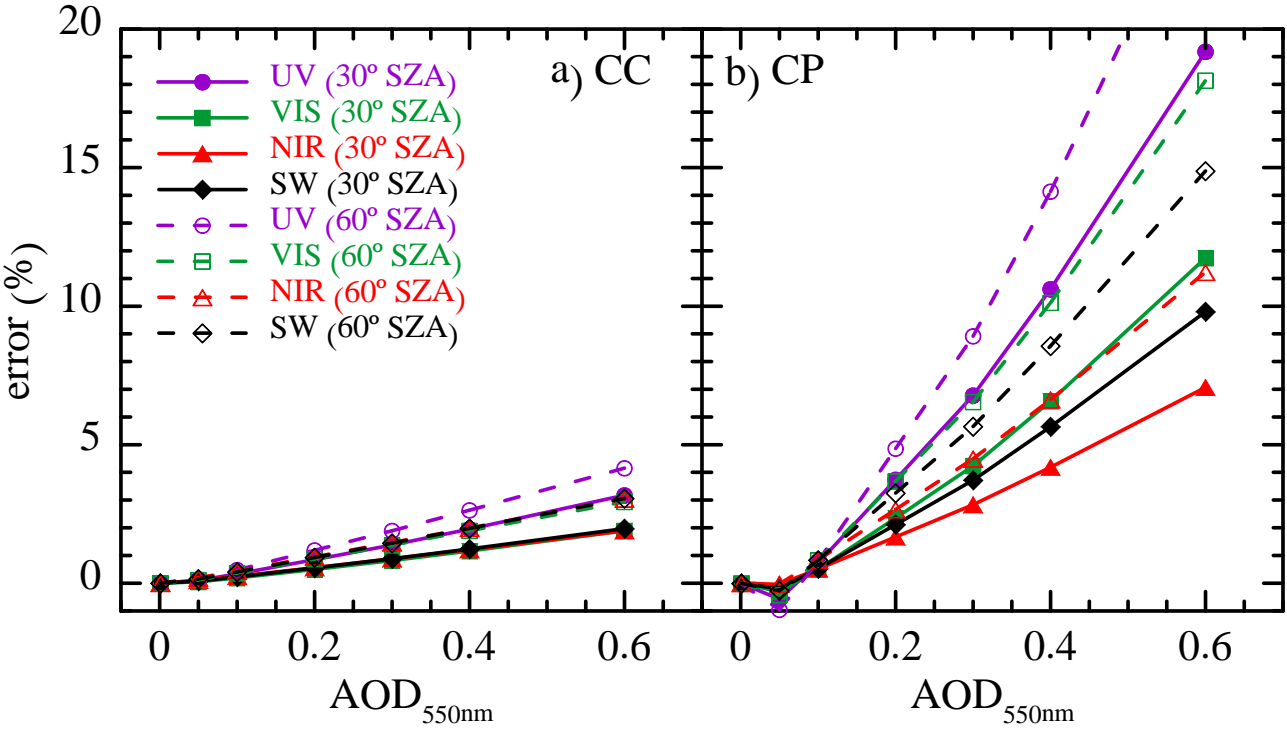**Figure 9.** Dependence of AFE$_{VIS}$/AFE$_{SW}$ (a, c, e) and AFE$_{NIR}$/AFE$_{SW}$ (b, d, f) ratios on SSA for

large (a, b), medium (c, d) and small (e, f) particles at the six sites: Barcelona (blue diamonds),

Palencia (purple triangles), Évora (red squares), Cabo da Roca (grey crosses), Granada (black stars),

and El Arenosillo (green circles).

974   Figure A1

975

976

977   Figure A1. Evolution of the error committed when the optical properties are fixed in the different

978   spectral range for two SZAs, and continental clean (CC, a) and continental polluted (CP, b)

979   aerosols.

980